Contract No:

This document was prepared in conjunction with work accomplished under Contract No. 89303321CEM000080 with the U.S. Department of Energy (DOE) Office of Environmental Management (EM).

Disclaimer:

A U.S. DEPARTMENT OF ENERGY NATIONAL LAB • SAVANNAH RIVER SITE • AIKEN, SC • USA

Analysis of Solids Obtained from 201O, 201P, 202A, and 202B Contactors in the Salt Waste Processing Facility

W. H. Woodham

April 2023

SRNL-STI-2023-00122, Revision 0

DISCLAIMER

Printed in the United States of America

Prepared for
U.S. Department of Energy

SRNL-STI-2023-00122
Revision 0

Keywords: *Solids, Salt, Mercury*

Retention: *Permanent*

Analysis of Solids Obtained from 201O, 201P, 202A, and 202B Contactors in the Salt Waste Processing Facility

W. H. Woodham

April 2023

Savannah River National Laboratory is operated by Battelle Savannah River Alliance for the U.S. Department of Energy under Contract No. 89303321CEM000080.

ACKNOWLEDGEMENTS

The author would like to thank Dee Wheeler, Haley Ramsey, and Leon Dyers for their work in handling and digesting solid samples within the SRNL Shielded Cells. Additionally, the author would like to recognize the efforts of Scott Brown, Sonia Dyer, Dave Diprete, Henry Ajo, and Catherine Housley for their roles in performing several analyses on these samples.

EXECUTIVE SUMMARY

In December 2022, Savannah River Mission Completion personnel recovered solids samples from four contactors (EXT-001, EXT-007, EXT-031, and EXT-040) employed at the Salt Waste Processing Facility (SWPF). These solids were submitted to Savannah River National Laboratory for analysis and characterization. This Technical Report outlines the analytical findings and observations associated with these samples and explores the potential source of solid generation within the SWPF.

The following conclusions are offered as a result of this work.

- The light color solids recovered from EXT-007 are consistent with crystallized, soluble salt components (such as sodium nitrate, sodium hydroxide, and sodium carbonate), all of which can be easily re-dissolved in process water and do not represent a threat to SWPF CSSX processing.
    - While the light solids from the top of EXT-040 were not analyzed, it is believed that they share similar characteristics to those recovered from EXT-007.
- The dark color solids recovered from EXT-001, EXT-031, and the inside of EXT-040 appear to be complex, consisting of several different types of solids:
    - High concentrations of mercury (Hg, 40-75% by mass) partially present as elemental Hg are consistent with the precipitation of Hg^0/Hg^{2+} from disproportionation of Hg^+ species in pH swing conditions.
    - Moderate concentrations of titanium (Ti) (2-7%, by mass) are also present, often co-located with Hg. This is consistent with co-precipitation, entrainment, and/or amalgamation of Ti with Hg.
    - Moderate concentrations of iron (Fe) (1-3%, by mass) are observed in SWPF solids and are likely attributable to erosion of stainless-steel components within the CSSX process.
    - Small concentrations of tungsten (W) and cobalt (Co) (<1%, by mass) are observed in SWPF solids. The presence of these solids is consistent with the erosion of components coated with W and Co (e.g., Stellite).
    - Small concentrations of aluminum (Al) (<1%, by mass) are observed in the form of gibbsite and potentially sodium aluminosilicate. The presence of these compounds is likely attributable to the pH swing observed between the scrub and extraction cycles within the CSSX process.

The following recommendations are made as a result of this work.

- Testing should be performed to determine the chemical drivers, process, and mechanism of Hg precipitation in CSSX processing. Special care should be taken to include titanium in tests to evaluate the potential for co-precipitation, entrainment, and amalgamation.
- Hg-mitigation options that would minimize or eliminate risks of Hg precipitation and solids accumulation (e.g., Hg-absorption techniques, ion exchange/adsorbents, flowsheet changes, etc.) should be assessed.

TABLE OF CONTENTS

LIST OF TABLES

LIST OF FIGURES

LIST OF ABBREVIATIONS

CSSX	Caustic Side Solvent Extraction
DMA	Direct Mercury Analysis
EDS	Energy Dispersive X-ray Spectroscopy
ICP-AES	Inductively Coupled Plasma-Atomic Emission Spectroscopy
MCU	Modular CSSX Unit
SEM	Scanning Electron Microscopy
SRMC	Savannah River Mission Completion
SRNL	Savannah River National Laboratory
SWPF	Salt Waste Processing Facility
SRS	Savannah River Site
XRD	X-ray Diffraction

1.0 Introduction

In December 2022, Savannah River Mission Completion (SRMC) personnel stationed at the Savannah River Site (SRS) Salt Waste Processing Facility (SWPF) recovered multiple samples of solids from centrifugal contactors employed in the BobCalix Caustic Side Solvent Extraction (CSSX) process during maintenance activities in 299-H. Samples were obtained from contactors EXT-001, EXT-031, EXT-040, and EXT-007 (employed as 202B, 202A, 201P, and 201O, respectively). These contactors are the four contactors surrounding the point in SWPF where scrub acid (0.05 M nitric acid) is combined with clarified salt solution (~5.6 M sodium salt solution). A flowchart describing the streams feeding each contactor is given in Figure 1-1. The red line indicates the flow of organic solvent used to extract Cs.

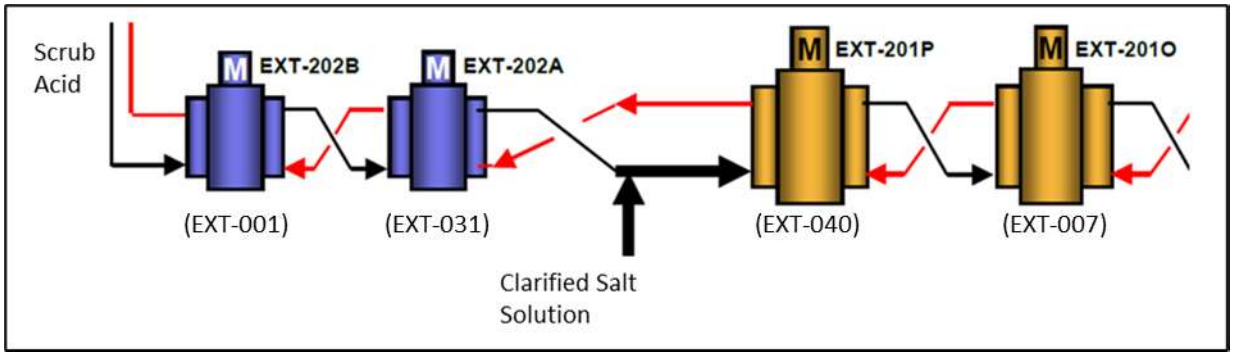

Figure 1-1. Process Flow Diagram of Contactors Yielding Solid Samples.

The presence of solids in the CSSX process (originally designed to be a liquid-only process) is problematic, as these solids may impede phase separation in the centrifugal contactors or occlude coalescer media downstream of the CSSX process. SRMC personnel packaged these solids samples and shipped them to Savannah River National Laboratory (SRNL) for subsequent analysis. The following analyses were requested by SRMC following SRNL receipt of these solids:[1]

- X-ray Diffraction (XRD) – to determine the crystallography of any species present.
- Scanning Electron Microscopy (SEM) – to physically observe the microscopic appearance of the solids. If possible, Energy Dispersive X-ray Spectroscopy (EDS) should be performed to determine chemical components in solids.
- Inductively Coupled Plasma Atomic Emission Spectroscopy (ICP-AES) – to determine total metal concentrations in solids.
- Direct Mercury Analysis (DMA) – to determine the amount of Hg present in these solids

The scope of this report is to analyze and discuss the results of the analyses performed on the solids obtained from the CSSX process. Recommendations for future work to understand the source of these solids in the SWPF are also provided.

2.0 Material Sampling and Analysis

2.1 Sample Acquisition and Handling

2.1.1 Sample Receipt into SRNL

Five samples of contactor solids were received into the SRNL Shielded Cells on December 22, 2022:

- ~7.5 g of dark solids obtained from EXT-031 (employed as scrub contactor 202A)[2]

- ~0.3 g of dark solids obtained from EXT-001 (employed as scrub contactor 202B)[2]
- ~17 g of light solids obtained from EXT-007 (employed as extraction contactor 201O)[3]
- ~5.3 g of light solids obtained from the "top" of EXT-040 (employed as extraction contactor 201P)[3]
- ~2.5 g of dark solids obtained from the "inside" of EXT-040

Samples were transferred from steel doorstops into glass vials for observation. Initial observations, results, and approximate sample masses were communicated to SRMC personnel. On January 4th, 2023, SRMC personnel approved the following handling and analytical activities:[4]

- Given the low amount of dark solids available from the EXT-001 sample, this material could be combined with solids obtained from EXT-031. Results from combined sample analysis will be reported as "202-A/B".
- The following analytical techniques were requested for "202-A/B", EXT-007 (201O), and the "inside sample of EXT-040 (201P):[4a]
    - ICP-AES (performed on solids digested via aqua regia or appropriate)
    - DMA (performed on solids digested via aqua regia or appropriate)
    - XRD (performed on as-received solids)
    - SEM (performed on as-received solids)
- The "top" sample from EXT-040 was requested to be withheld from analysis. The light color and location of sample acquisition indicated salt presence to SRMC personnel. EXT-040-Top was therefore not considered a priority for analysis.

Pictures of each sample are given in Figure 2-1.

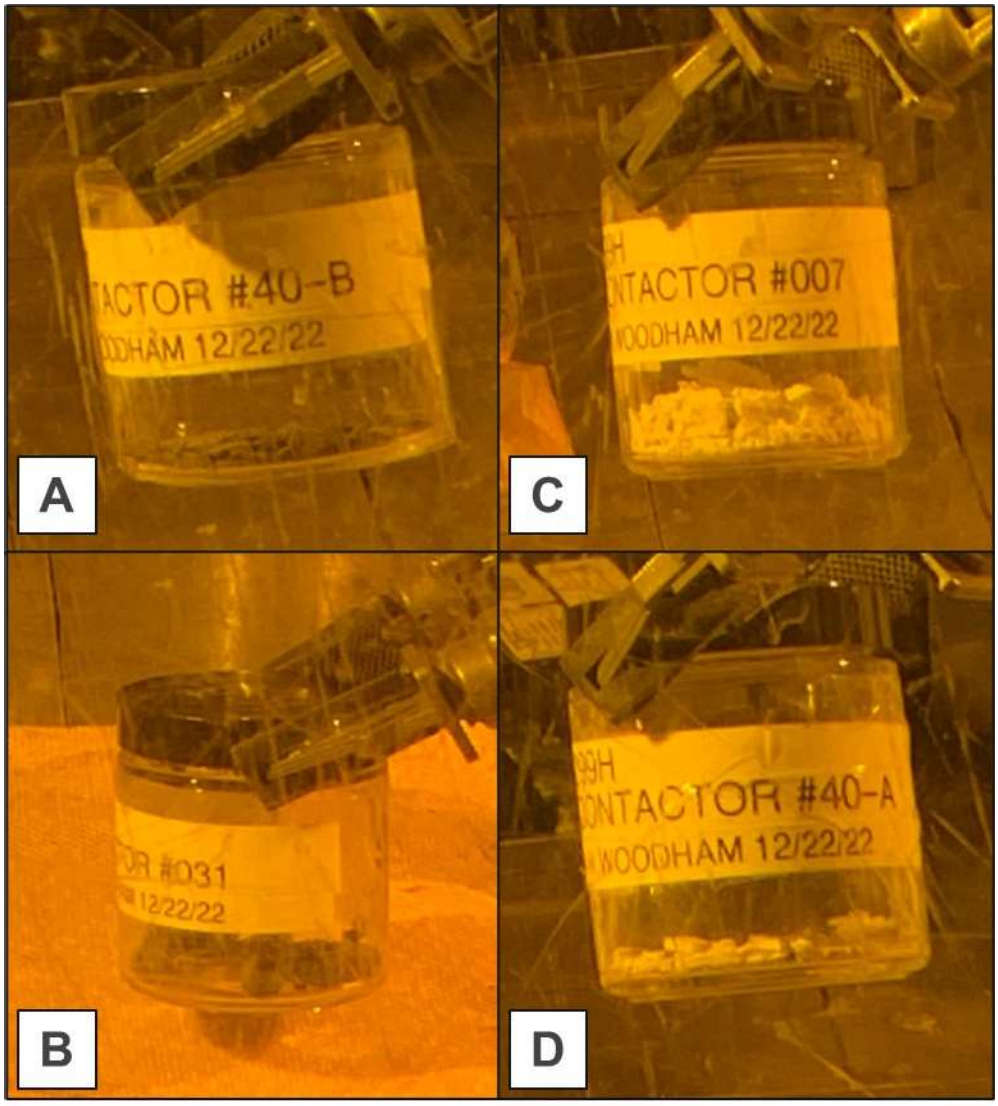

Figure 2-1. Photographs of Solids Samples Received from SWPF. A) Solids from EXT-040-Inside. B) Combination of solids from EXT-001 and EXT-031 (referred to as 202-A/B). C) Solids from EXT-007. D) Solids from EXT-040-Top.

Upon receipt in the SRNL Shielded Cells, it was observed that dose rates from solids samples (particularly dark solids from EXT-031) exceeded hood limits for handling outside of the Shielded Cells (which may have impacted analysis via XRD and SEM). In an effort to keep dose as low as reasonably achievable (per SRS Manual SCD-6),[5] additional analyses were requested to determine dose rates of samples.

- GammaScan – to determine the amount of gamma radiation produced from each sample
- Liquid Scintillation – to determine the amount of alpha and beta radiation produced from each sample
- Cs-removed Liquid Scintillation – to determine the amount of non-cesium beta radiation produced from each sample

With dose rates both provided and communicated to XRD and SEM-EDS staff, solid samples were submitted for XRD and SEM-EDS to ensure dose to personnel remained ALARA.

2.1.2 Solid Dissolution Using In-Cells Digestion Techniques

In order to submit samples of solids obtained from contactors for analysis by ICP-AES, DMA, and radiation dose, solids had to first be converted into an aqueous solution via digestion. This was first attempted via aqua regia digestion within the SRNL Shielded Cells. Following the addition of aqua regia and heating, solids persisted from the 202-A/B and EXT-040-Inside samples. No persistently insoluble solids were visible from the EXT-007 sample, qualitatively indicating full dissolution. The aqua regia-digested samples were submitted for preliminary DMA, ICP-AES, Gamma Scan, Liquid Scintillation, and Cs-removed Liquid Scintillation.

Additional digestions were then authorized to enhance the accuracy of metal concentrations in the 202-A/B and EXT-040-Inside solids:

- Peroxide fusion was performed on dark solids. Generated samples were submitted for ICP-AES.
- The peroxide fusion technique is not recommended for mercury analysis due to the high temperatures employed. Therefore, a special preparation using nitric and sulfuric acids was employed per recommendation of SWPF chemists. Generated samples were submitted for DMA.

Results from both preliminary (aqua regia) and final (peroxide fusion/nitric-sulfuric) digestions are presented in this report for discussion.

2.2 Quality Assurance

Requirements for performing reviews of technical reports and the extent of review are established in manual E7 2.60.[6] SRNL documents the extent and type of review using the SRNL Technical Report Design Checklist contained in WSRC-IM-2002-00011, Rev. 2. A request for work via Technical Assistance Request (TAR) necessitates a functional classification of Production Support or lower. Per Manual E7, Procedure 3.60, a technical report supporting a functional classification of Production Support requires a technical review by Design Check.[7] A Design Check was performed on this report in accordance with the requirements outlined in Manual E7, Procedure 2.60.[6]

3.0 Results and Discussion

3.1 Analysis of EXT-007 (Extraction Contactor) Solids

3.1.1 Elemental Analysis of EXT-007 Solids

The measured elemental composition of EXT-007 solids is given in Table 3-1. Values for mercury concentration were measured by DMA, while remaining metals were measured via ICP-AES.

Table 3-1. Elemental Analysis of EXT-007 Solids.

Element	Concentration (mg kg^{-1})	Element	Concentration (mg kg^{-1})
Ag	< 8.70	Mn	< 4.41
Al	6,120	Mo	20.8
B	42.5	Na	240,000
Ba	< 0.711	Ni	13.3
Be	< 0.188	P	143
Ca	305	Pb	< 2.63
Cd	< 0.206	S	10,100
Ce	< 16.2	Sb	< 31.5
Co	< 1.02	Si	< 42.3
Cr	103	Sn	< 16.5
Cu	< 6.42	Sr	< 1.15
Fe	122	Th	< 22.5
Gd	< 1.12	Ti	37.6
Hg	701	U	< 11.0
K	440	V	< 10.9
La	< 0.611	Zn	< 8.83
Li	< 57.5	Zr	< 0.993
Mg	49.0		

The results in Table 3-1 are consistent with that of sodium salts. The largest component observed was sodium at ~24%. Approximately 1% sulfur is present (likely as sulfate), along with ~0.6% Al. Approximately (701 ppm Hg was observed in these solids, which is significantly less than other elements. It should be noted that the amount of detectable Hg might vary significantly between samples due to sampling bias.

3.1.2 X-Ray Diffraction Analysis of EXT-007 Solids

The XRD spectrum observed from EXT-007 solids is given in Figure 3-1.

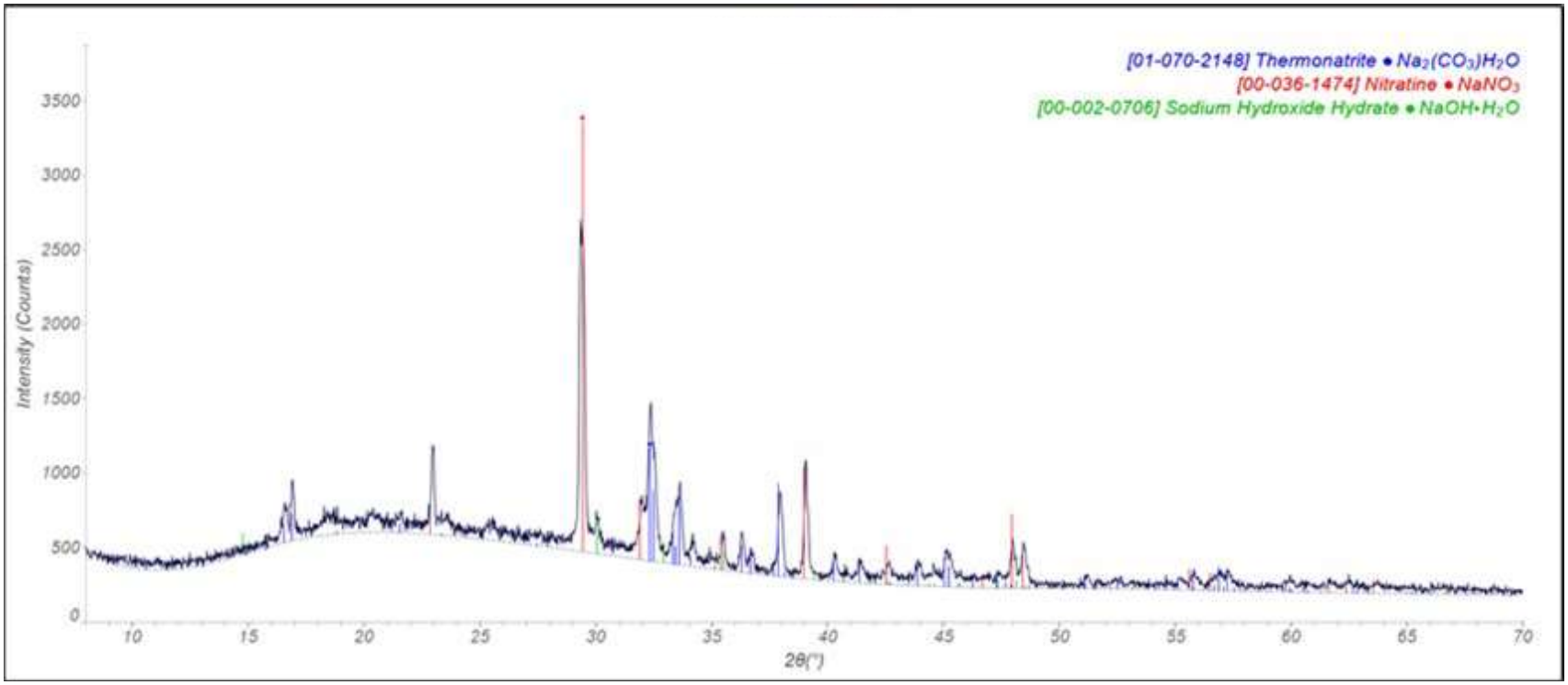

Figure 3-1. XRD Analysis of EXT-007 Solids.

The XRD spectrum in Figure 3-1 is consistent with a blend of sodium salts. Species such as sodium carbonate (Na_2CO_3), sodium nitrate ($NaNO_3$), and sodium hydroxide (NaOH) are most dominant in the spectrum. This information, combined with the elemental analysis in Table 3-1 suggests that the EXT-007 solids are mostly salt-based and are likely water-soluble and likely formed from residual salt solution that evaporated.

3.1.3 Scanning Electron Microscopic Analysis of EXT-007 Solids

3.1.3.1 Large Area Scan

A large-area SEM image of EXT-007 solids is given in Figure 3-2. The scale (reported in lower left of image) is set at 2.5 mm, for reference. An EDS scan of the region outlined in white is presented in Figure 3-3.

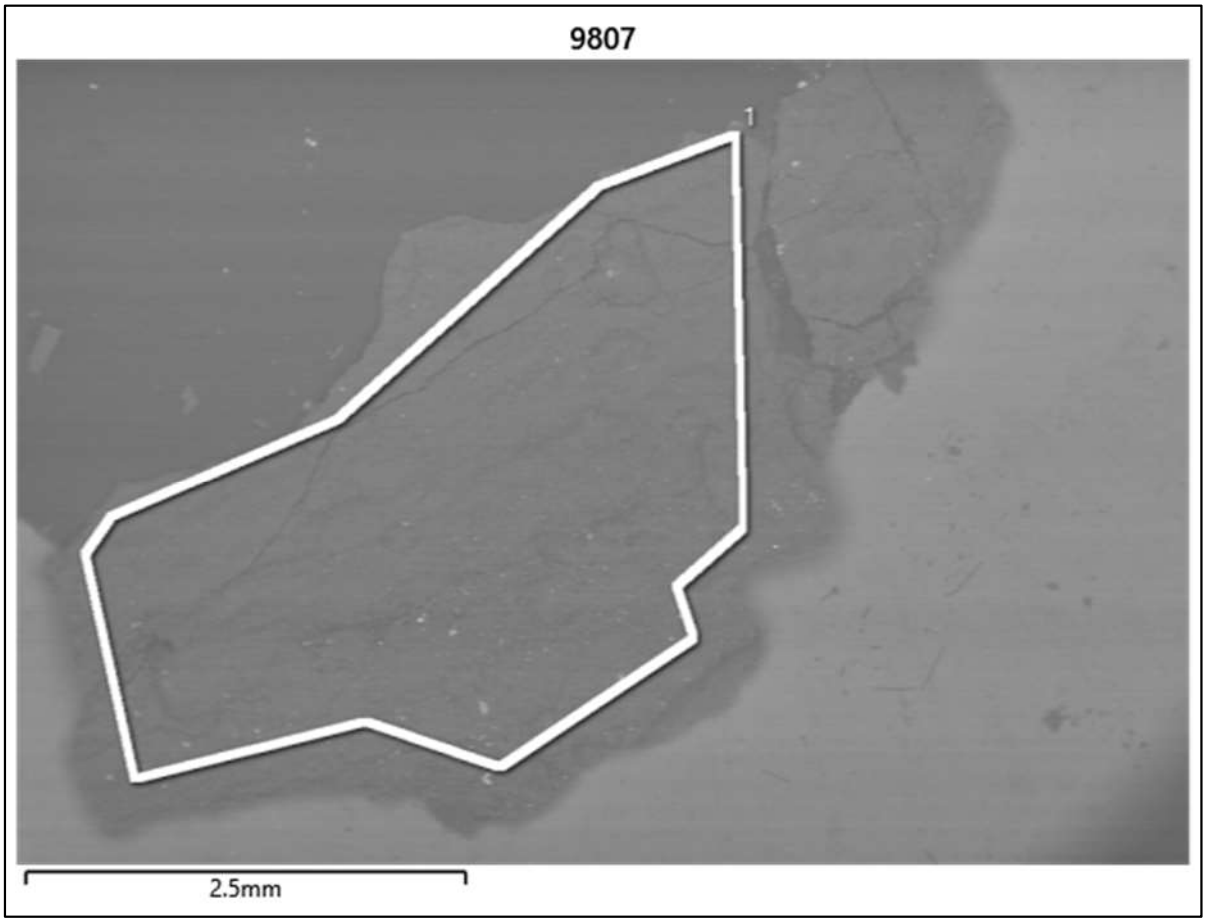

Figure 3-2. Large Area SEM Image of EXT-007 Solids.

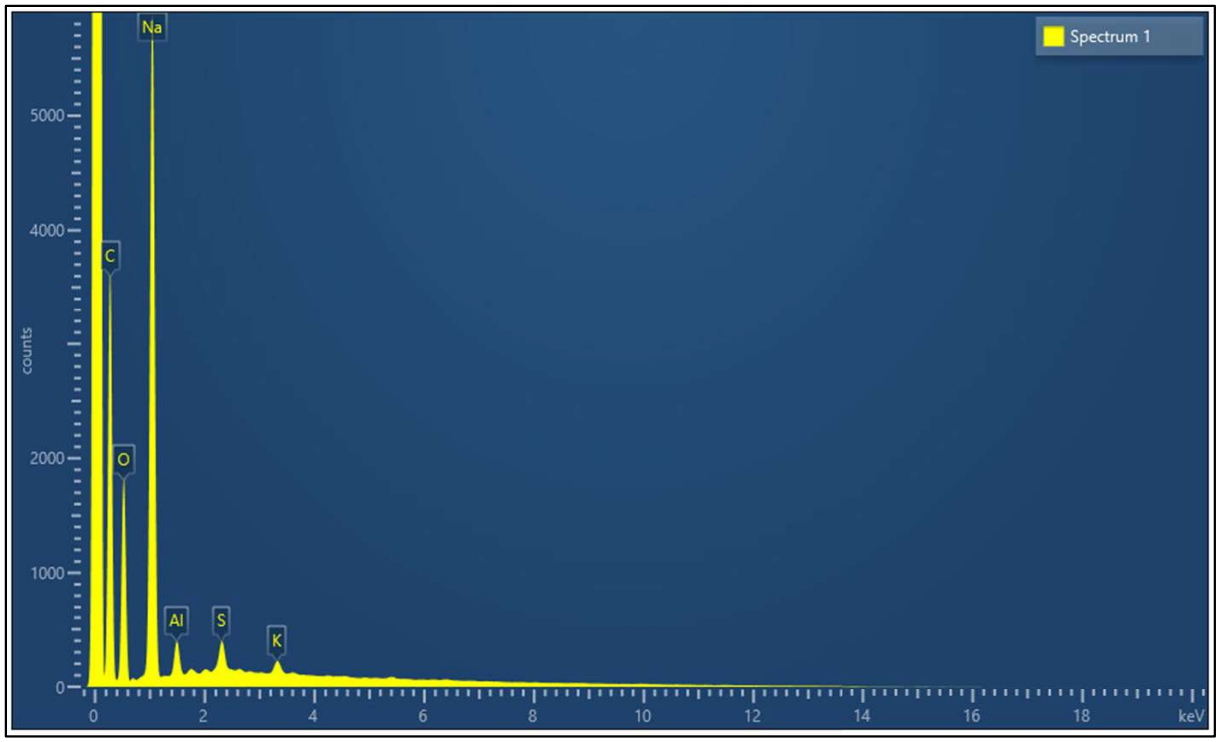

Figure 3-3. Large Area EDS Scan of EXT-007 Solids.

The large area EDS scan in Figure 3-3 indicates the presence of elements typically associated with salt species (Na, O, Al, S, K). Note that the carbon peak in EDS spectra is not necessarily representative of elemental make-up, as carbon tape is used as an adhesive to hold the sample in place and a carbon coating is applied to minimize charging during analysis. The EDS spectra agrees with prior observations that EXT-007 solids are mostly salt-based.

3.1.3.2 Low-Magnification Scan

A low-magnification SEM image of EXT-007 solids is given in Figure 3-4. Note that the reference scale given in 250 µm. Additionally, EDS spectra of regions 1 and 2 are given in Figure 3-5 and Figure 3-6, respectively.

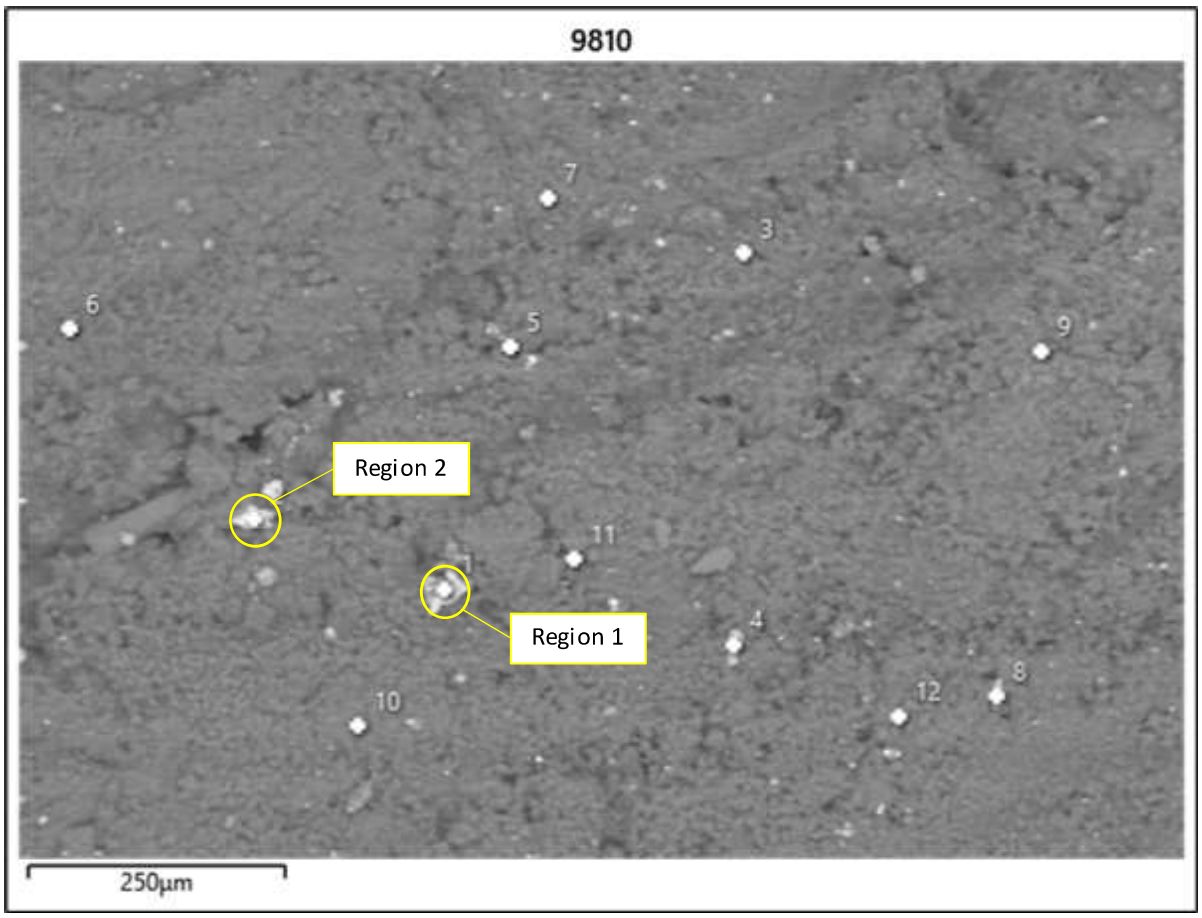

Figure 3-4. Low-Magnification SEM Image of EXT-007 Solids.

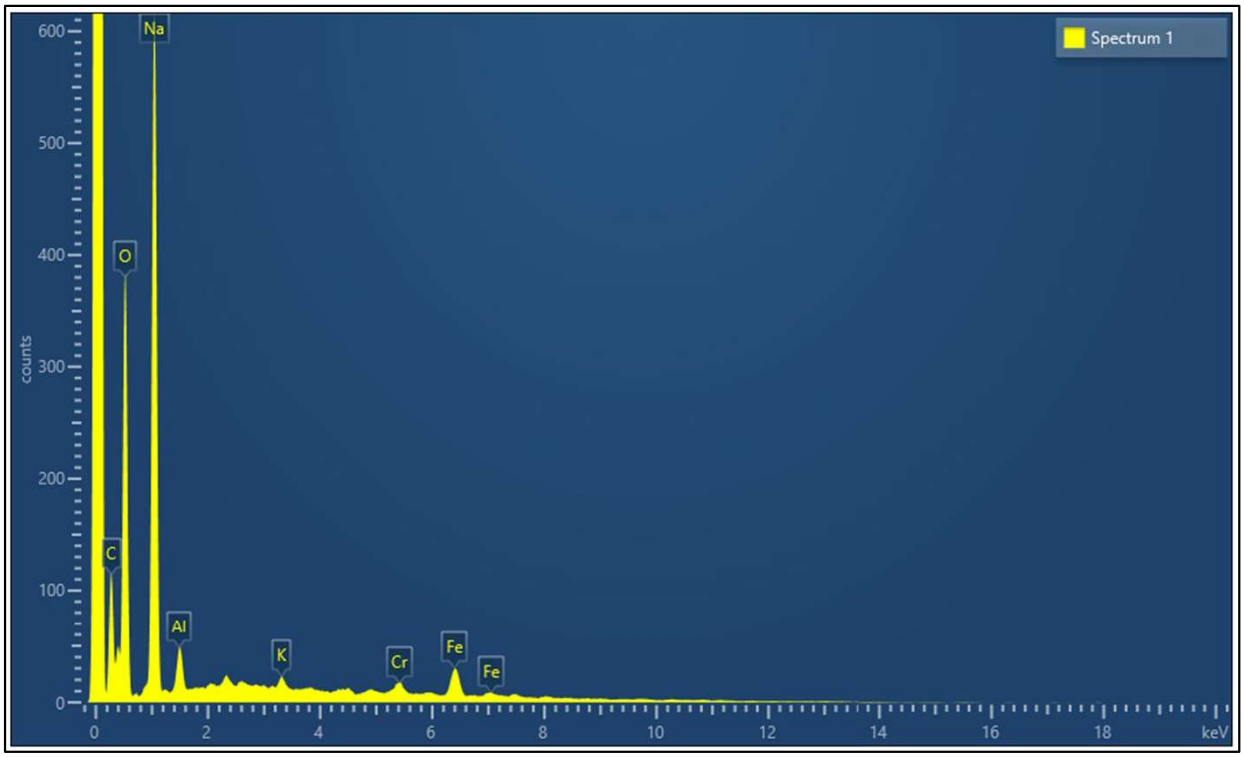

Figure 3-5. EDS Spectrum of Region 1 in Low-Magnification EXT-007 SEM Image.

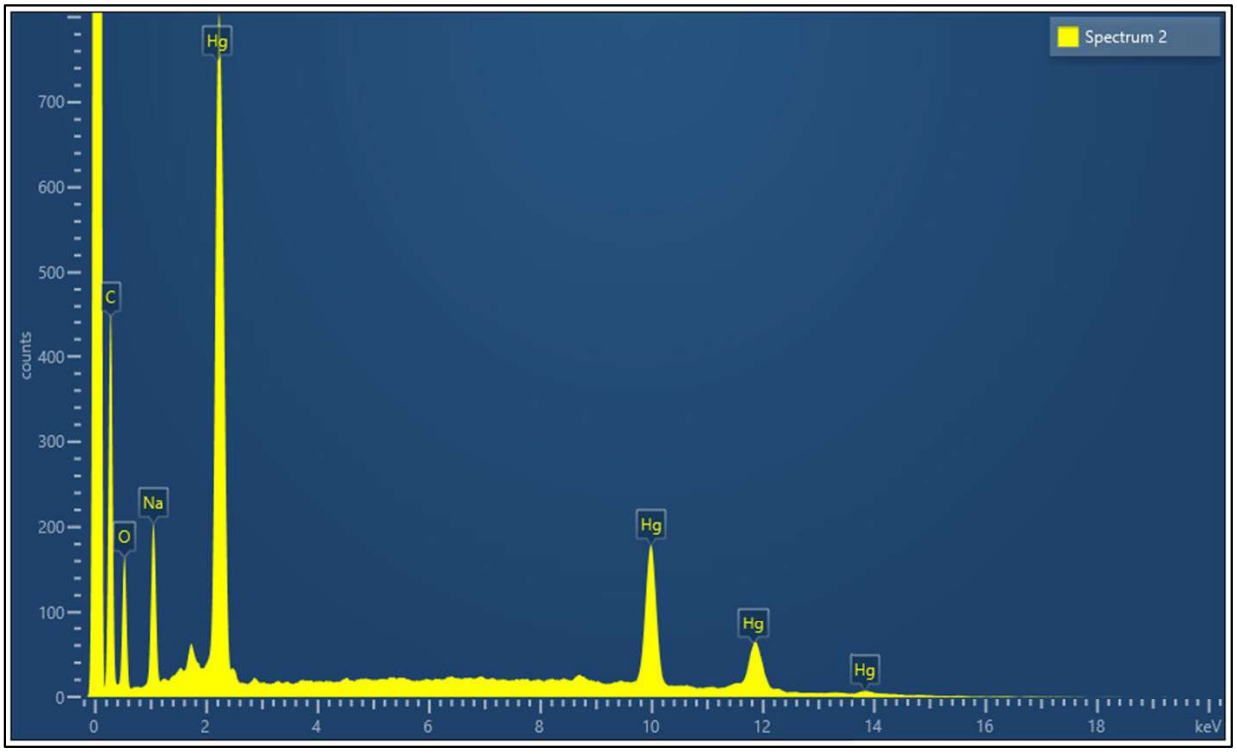

Figure 3-6. EDS Spectrum of Region 2 in Low-Magnification EXT-007 SEM Image.

The EDS spectra given in Figure 3-5 and Figure 3-6 indicate the presence of solids composed of Fe, Cr, and Hg. However, given that the EDS spectrum of the large area scan (Figure 3-3) does not yield these peaks, these elements are likely to be present in only trace amounts. This is consistent with the concentrations of each element reported in Table 3-1.

3.1.3.3 High-Magnification Scan

A high-magnification SEM image of EXT-007 solids is given in Figure 3-7. Note that the reference scale given is 25 µm. Additionally, an EDS spectrum of region 3 is given in Figure 3-8.

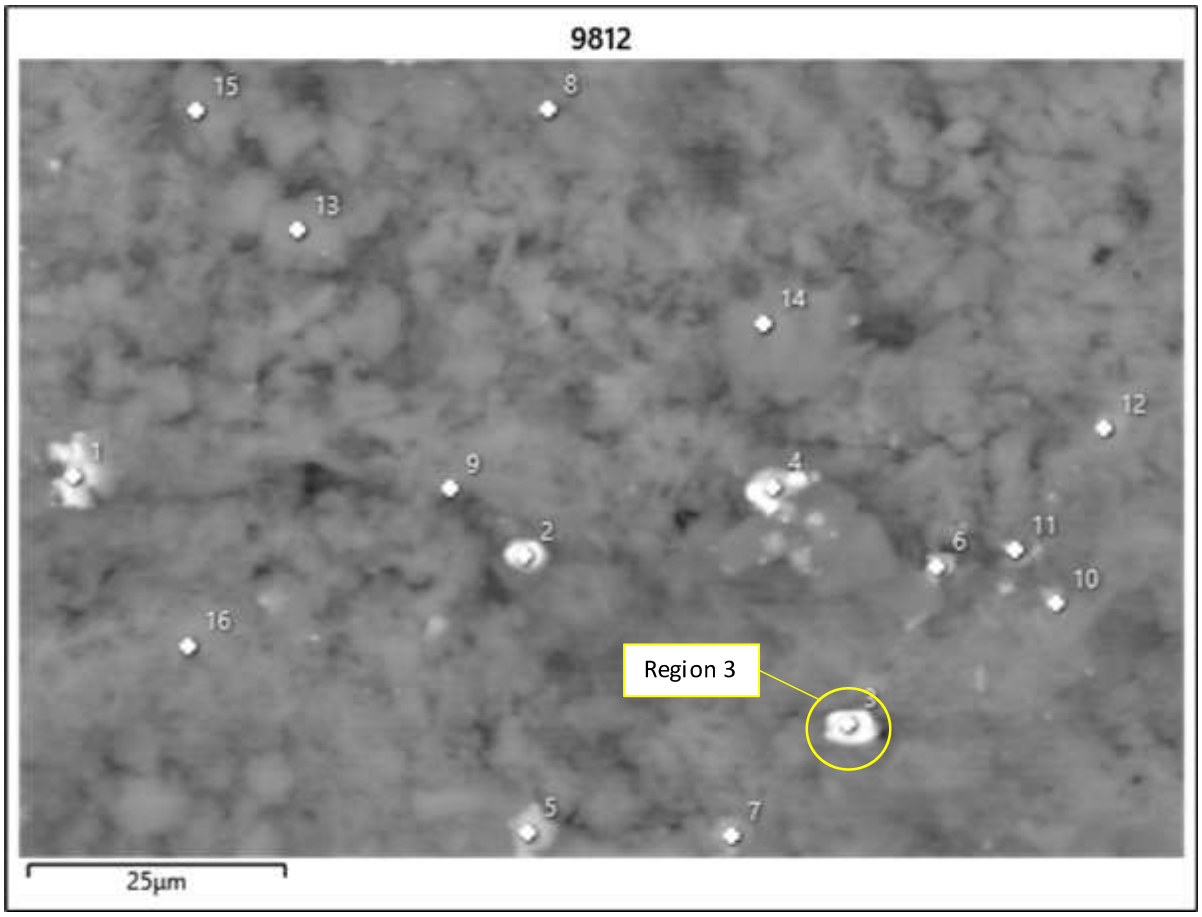

Figure 3-7. High-Magnification SEM Image of EXT-007 Solids.

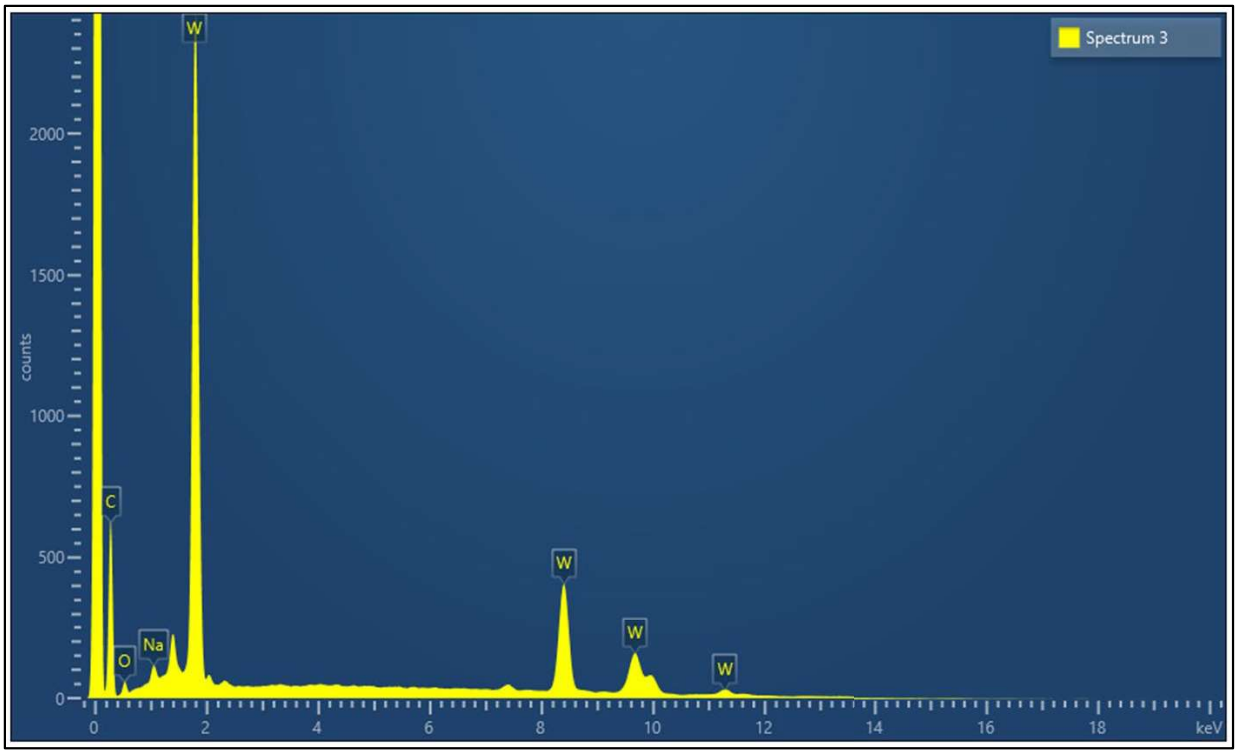

Figure 3-8. EDS Spectrum of Region 3 in High-Magnification EXT-007 Solids SEM Image.

The EDS spectrum of region 3 indicates a significant localized presence of tungsten. Inspection of the particle size associated with region 3 in Figure 3-7 indicates that this tungsten-rich particle is approximately 3-5 µm in size. This indicates that tungsten-rich particles, though rare, do appear in EXT-007 solids. The size indicated by SEM suggests that these particles might be generated downstream of the alpha strike filters in SWPF.

3.2 Analysis of EXT-040-Inside (Extraction Contactor) Solids

3.2.1 Elemental Analysis of EXT-040-Inside Solids

Elemental analysis of EXT-040-Inside solids is given in Table 3-2. Values in the second column are reported from an incomplete dissolution by aqua regia. Values in the third column are reported from a special preparation using nitric and sulfuric acids (Hg) and peroxide fusion (other elements). Values reported in the fourth column are recommended as "best values", taken from both data sets to be as accurate as possible. Preference is given to lower detection limits, when available. In cases where only one technique yielded a reportable concentration, that measured concentration is reported as a best estimate. In cases where both techniques yielded reportable quantities, the larger concentration is reported due to potential issues with insolubility. In the case of Hg, no observable benefit from special preparation was observed. Therefore, best estimates for Hg are reported as the average of the two techniques. Note that separate samples are submitted for DMA and ICP-AES. For this reason, sampling bias exists that may impact the ability to demonstrate complete mass balance closure.

Table 3-2. Elemental Analysis of EXT-040-Inside Solids.

Element	Concentration (Aqua Regia) (mg kg^{-1})	Concentration (Peroxide Fusion/Special Prep.) (mg kg^{-1})	Best Value (mg kg^{-1})
Ag	< 7.41	< 668	< 7.41
Al	1,800	7,280	7,280
B	< 16.6	< 53.8	< 16.6
Ba	33.5	< 50.6	33.5
Be	< 0.160	< 4.33	< 0.160
Ca	740	NR†	740
Cd	8.03	< 8.61	8.03
Ce	< 13.8	< 810	< 13.8
Co	1,220	1,210	1,220
Cr	2,930	4,910	4,910
Cu	74.4	< 135	74.4
Fe	14,600	21,500	21,500
Gd	< 0.952	< 25.7	< 0.952
Hg	752,000	610,000‡	681,000
K	< 176	< 2,500	< 176
La	< 0.520	< 12.0	< 0.520
Li	< 48.9	< 333	< 48.9
Mg	171	285	285
Mn	226	402	402
Mo	126	235	235
Na	7,620	NR†	7,620
Ni	1,410	2,020	2,020
P	< 5.80	< 332	< 5.80
Pb	77.0	< 207	77.0
S	393	< 830	393
Sb	< 26.8	< 235	< 26.8
Si	342	5,520	5,520
Sn	< 14.0	< 378	< 14.0
Sr	6.19	< 22.6	6.19
Th	< 19.2	< 516	< 19.2
Ti	19,500	50,300	50,300
U	164	< 252	164
V	< 9.26	< 77.3	< 9.26
Zn	50.8	< 100	50.8
Zr	12.4	NR†	12.4

†The peroxide fusion technique involves the use of sodium peroxide in a zirconium crucible. For this reason, Na and Zr measurements by peroxide fusion are unreliable and are therefore not reported. Additionally, a calcium impurity was observed in the blank sample, suggesting that calcium observed in the peroxide fusion sample may be a result of trace impurities in sodium peroxide. Therefore, Ca is not reported via peroxide fusion.
‡The mercury value reported in the third column is taken from the special preparation using nitric and sulfuric acids. The temperatures employed in peroxide fusion are prohibitive for effective Hg analysis.

The elemental analysis given in Table 3-2 yields several interesting observations. Mercury appears to make-up the bulk of the solids mass, with ~68.1% Hg (by mass). The difference between these two measurements is likely attributable to sampling bias (instead of decreased solubility via special preparation). Additionally, iron and titanium make up an appreciable fraction of the remaining solids (2.15% and 5.03% by mass, respectively). These results indicate that the majority of the EXT-040-Inside solids are composed of metal species. Furthermore, the increased solubility of aluminum and silicon when employing peroxide fusion

(7,280 and 5,520 ppm) compared to that observed in aqua regia (1,800 and 342 ppm) might suggest the presence of insoluble aluminum species (such as aluminum hydroxide or sodium aluminosilicate).

3.2.2 X-Ray Diffraction Analysis of EXT-040-Inside Solids

X-ray diffraction spectra for EXT-040-Inside solids are given in Figure 3-9 and Figure 3-10.

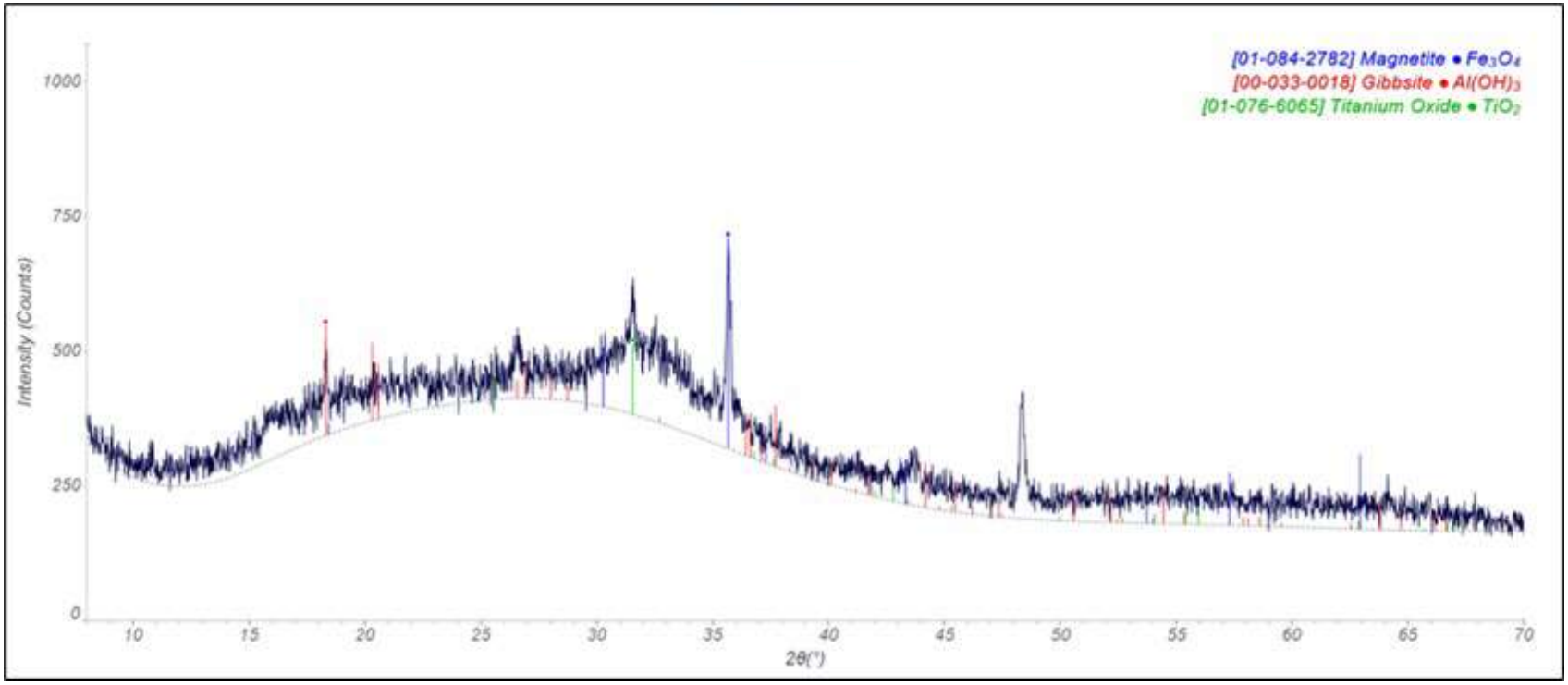

Figure 3-9. XRD Analysis of EXT-040-Inside Solids.

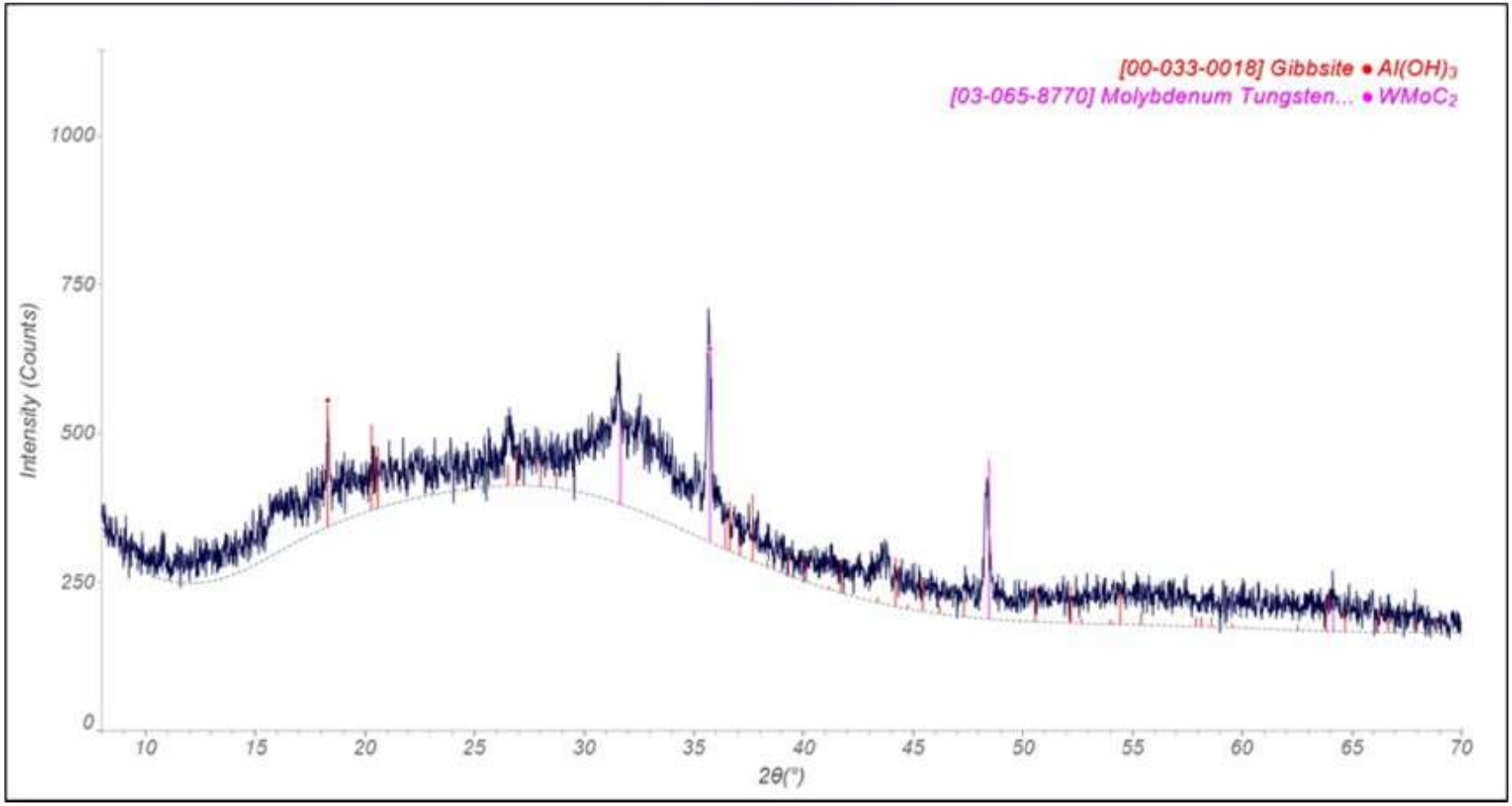

Figure 3-10. Alternative XRD Analysis of EXT-040-Inside Solids.

The XRD analyses for EXT-040-Inside solids given in Figure 3-9 and Figure 3-10 suggest that the solids from EXT-040 are largely amorphous with little sign of crystallinity. Figure 3-9 indicates the presence of Gibbsite (aluminum hydroxide) as well as traces of magnetite (iron oxide) and titanium oxide (in this analysis, a single peak at ~48° remains uncharacterized). However, an alternate XRD analysis of EXT-040-Inside solids (given in Figure 3-10) indicates that molybdenum tungsten carbide is capable of producing the unknown peak at 48° as well as the peaks previously identified as iron oxide and titanium oxide. The presence of Fe, Ti, Mo, and W (confirmed in discussions above) indicate that either analysis is possibly correct, suggesting that the XRD technique is inconclusive for species other than Gibbsite in the case of EXT-040-Inside solids.

3.2.3 Scanning Electron Microscopic Analysis of EXT-040-Inside Solids

3.2.3.1 Large Area Scan

A large area SEM image of EXT-040-Inside solids is given in Figure 3-11. An EDS spectrum for the region outlined in white is provided in Figure 3-12. The scale used for reference in the image is 2.5 mm.

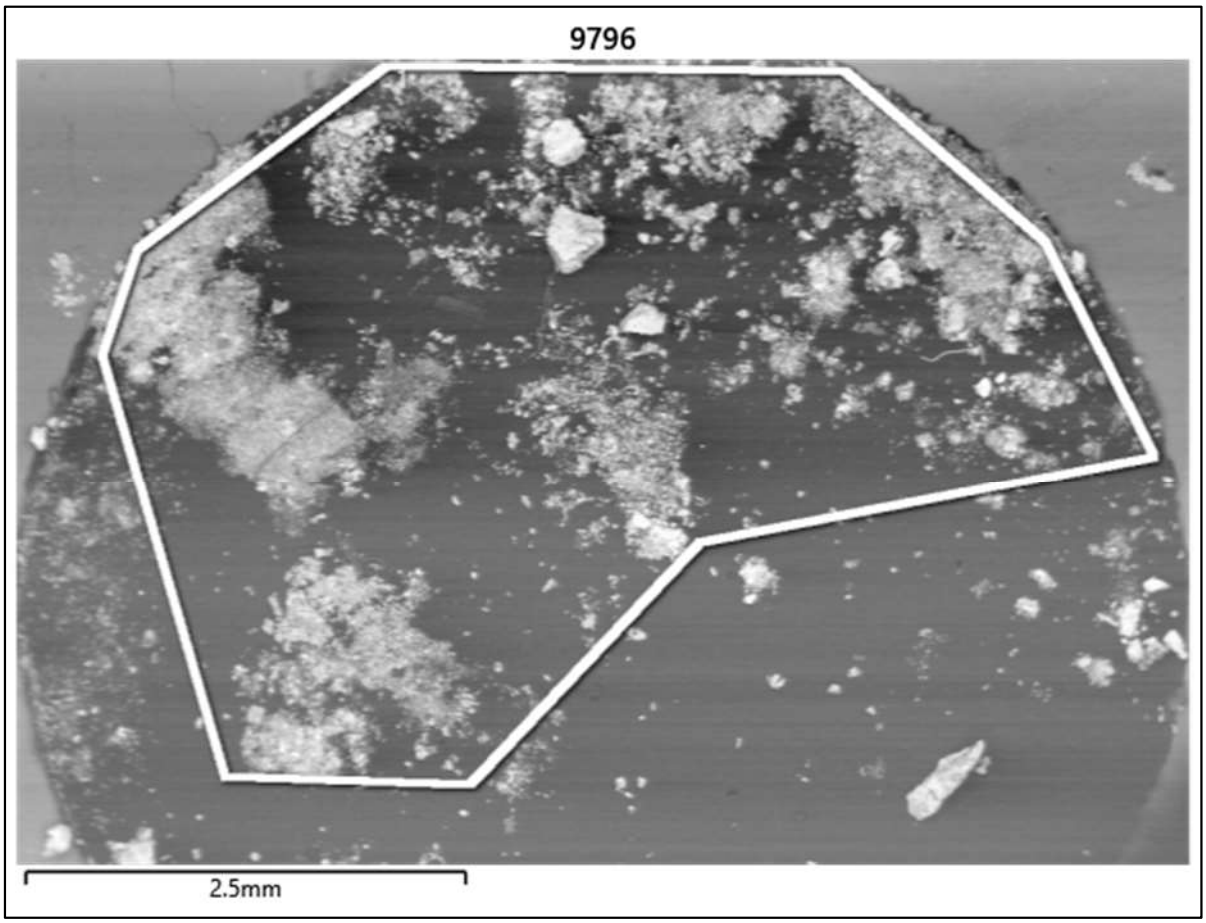

Figure 3-11. Large Area SEM Image of EXT-040-Inside Solids.

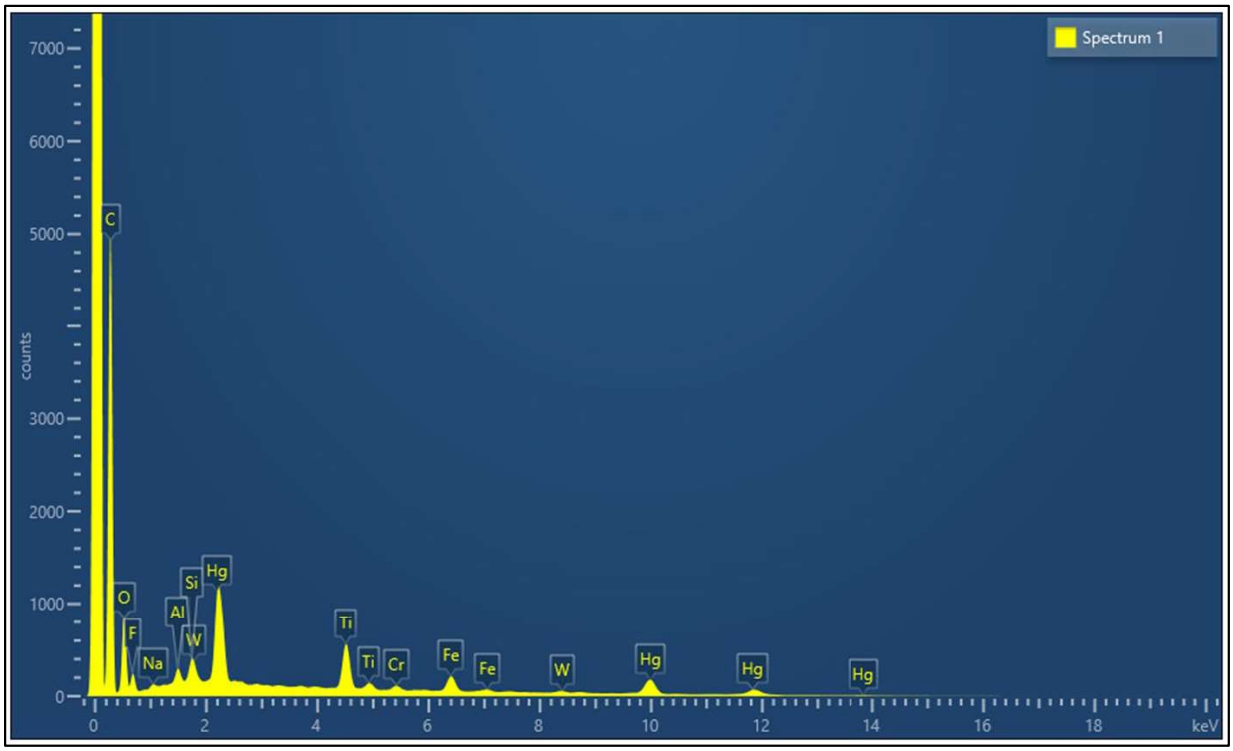

Figure 3-12. Large Area EDS Scan of EXT-040-Inside Solids.

The large area EDS scan for EXT-040-Inside solids (shown in Figure 3-12) indicates the presence of several metals, including Na, Al, W, Si, Hg, Ti, Cr, and Fe. The presence of these metals is consistent with SEM-EDS spectra taken from previous SWPF solids samples. The spectrum above also shows evidence of the presence of fluorine, an element most closely associated with Cs-7SB modifier within SWPF. The appearance of F might suggest a small presence of solvent-related components or degradation products.

3.2.3.2 Low-Magnification Scan

A low-magnification SEM image of EXT-040-Inside solids is given in Figure 3-13. The scale used for reference in the image is 250 µm. EDS spectra for various regions within the image are given in Figure 3-14, Figure 3-15, Figure 3-16, and Figure 3-17.

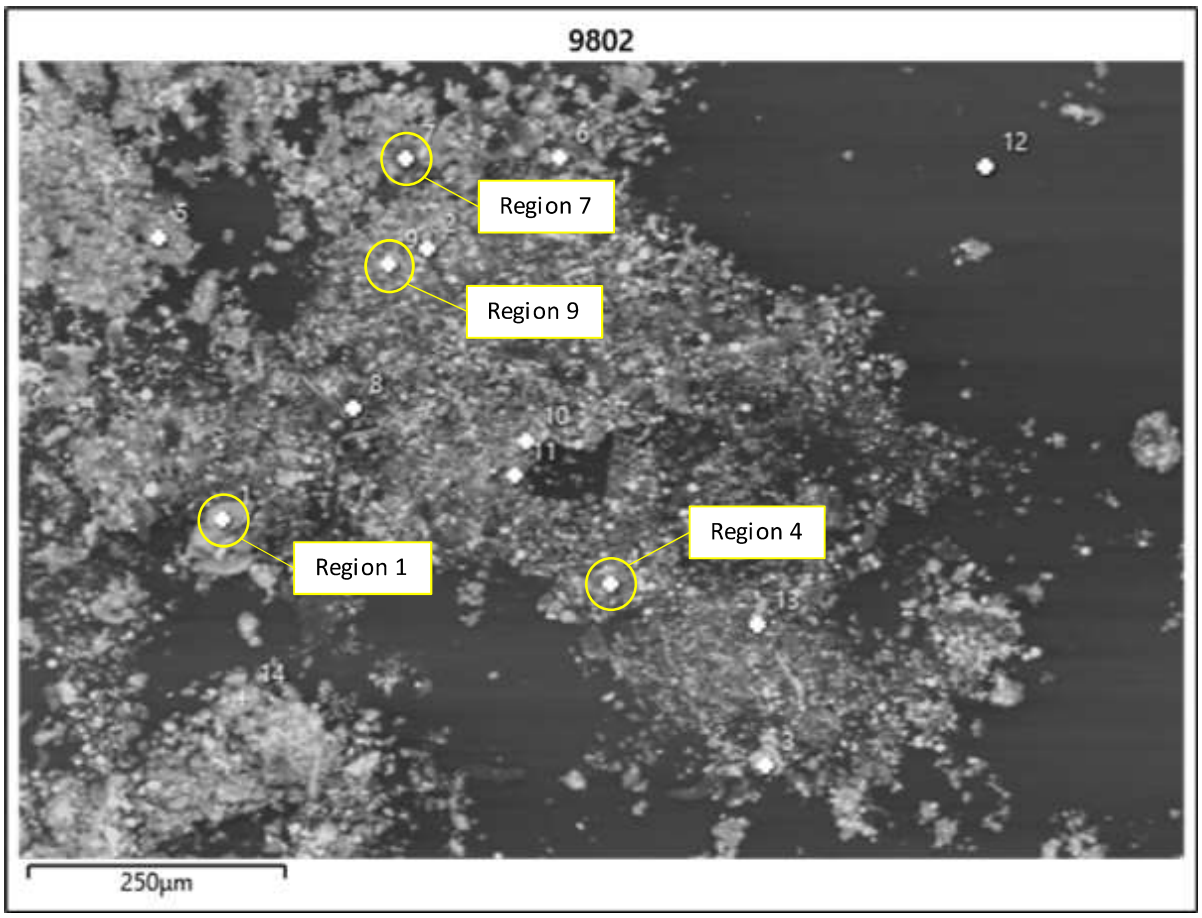

Figure 3-13. Low-Magnification SEM Image of EXT-040-Inside Solids.

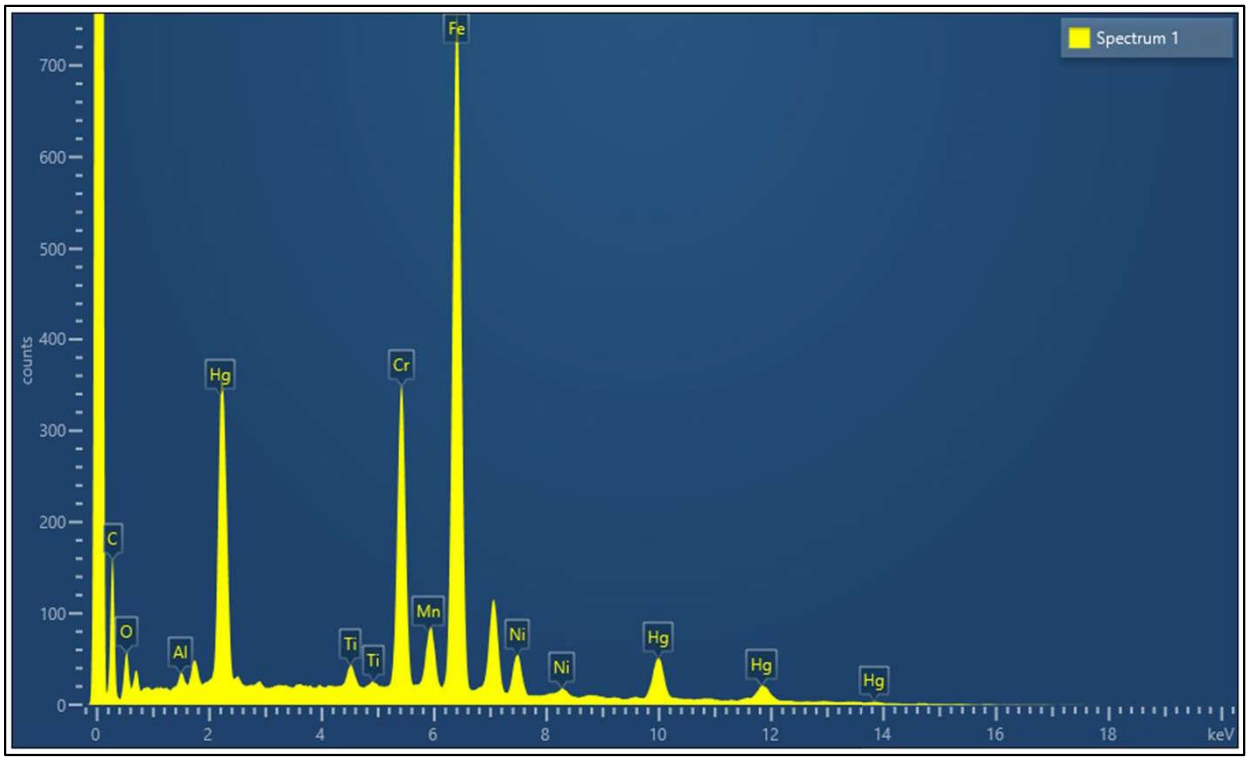

Figure 3-14. EDS Spectrum of Region 1 in Low-Magnification EXT-040-Inside Solids SEM Image.

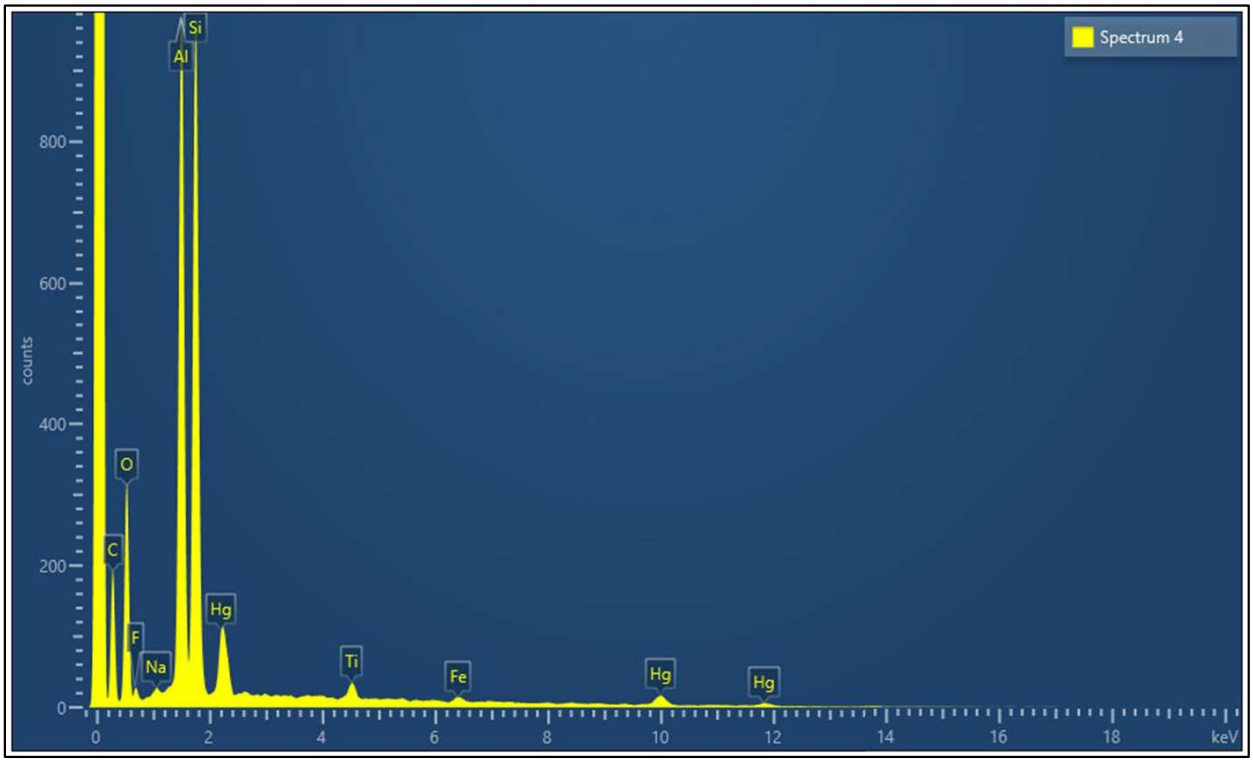

Figure 3-15. EDS Spectrum of Region 4 in Low-Magnification EXT-040-Inside Solids SEM Image.

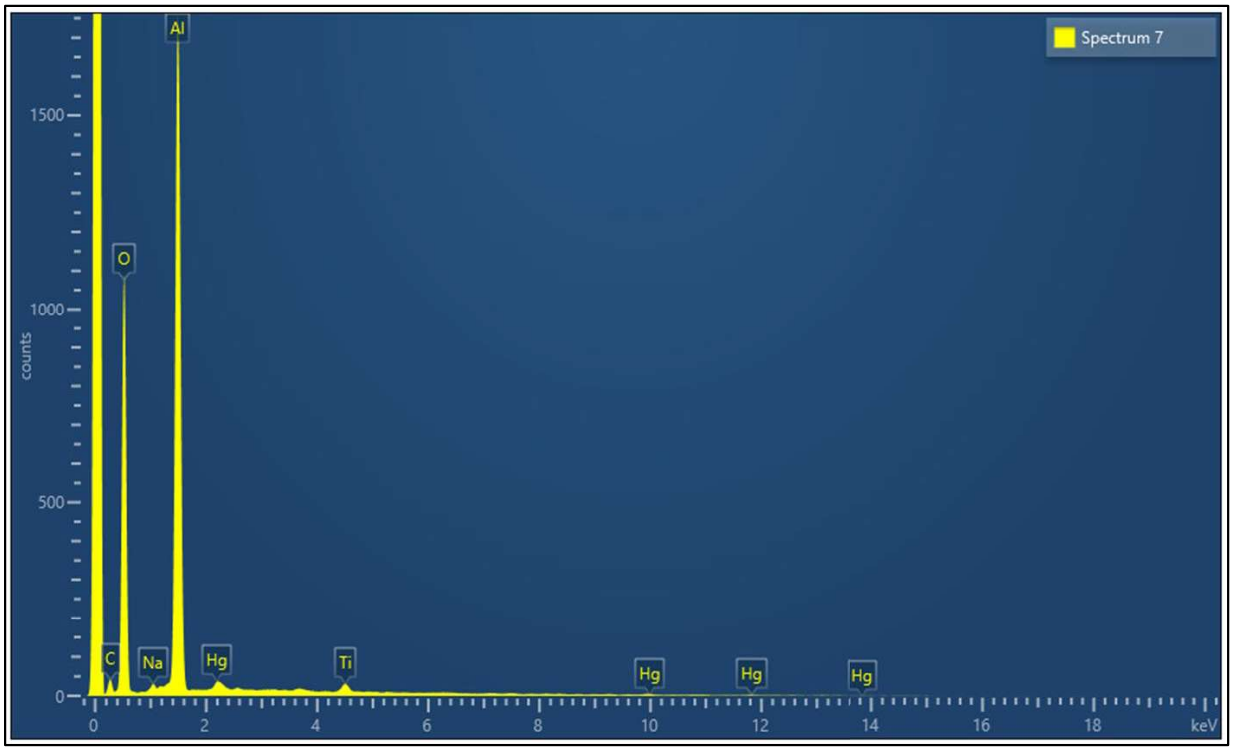

Figure 3-16. EDS Spectrum of Region 7 in Low-Magnification EXT-040-Inside Solids SEM Image.

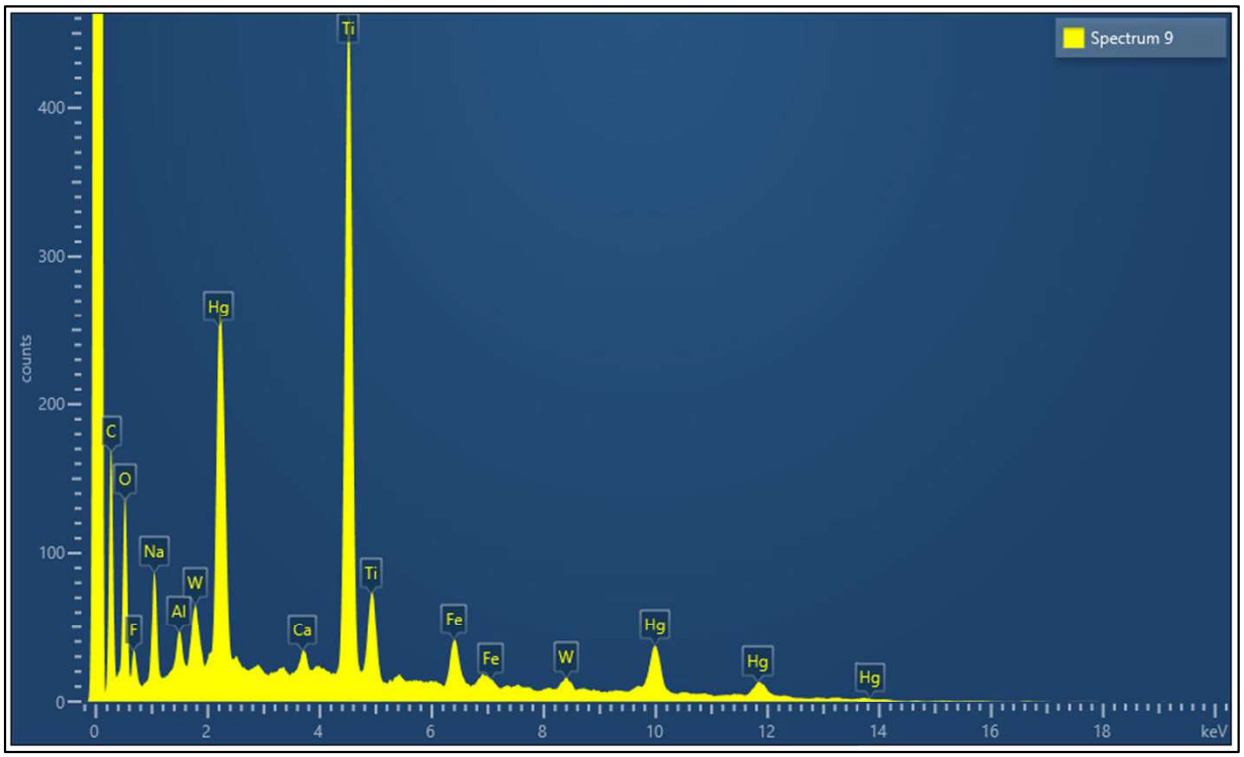

Figure 3-17. EDS Spectrum of Region 9 in Low-Magnification EXT-040-Inside Solids SEM Image.

The EDS spectra in Figure 3-14 show a relatively large amount of iron, chromium, manganese, and nickel co-located within region 1. The appearance of these species co-located may indicate the presence of ferrous alloy particles within the EDS region. Similarly, the appearance of aluminum/silicon and aluminum in regions 4 and 7 (Figure 3-15 and Figure 3-16, respectively) may indicate the presence of aluminum-containing species (such as Gibbsite or sodium aluminosilicate). Finally, an EDS spectrum of region 9 within the SEM image (given in Figure 3-17) yielded large peaks of titanium and mercury. The differences in elemental composition across different regions indicate the presence of different types of solids, which may further emphasize the potential for sampling bias when handling SWPF solids.

3.2.3.3 High-Magnification Scan

A high-magnification SEM image of EXT-040-Inside solids is given in Figure 3-18. The scale used for reference in the image is 25 µm. EDS spectra for various regions within the image are given in Figure 3-19, Figure 3-20, Figure 3-21, Figure 3-22, and Figure 3-23.

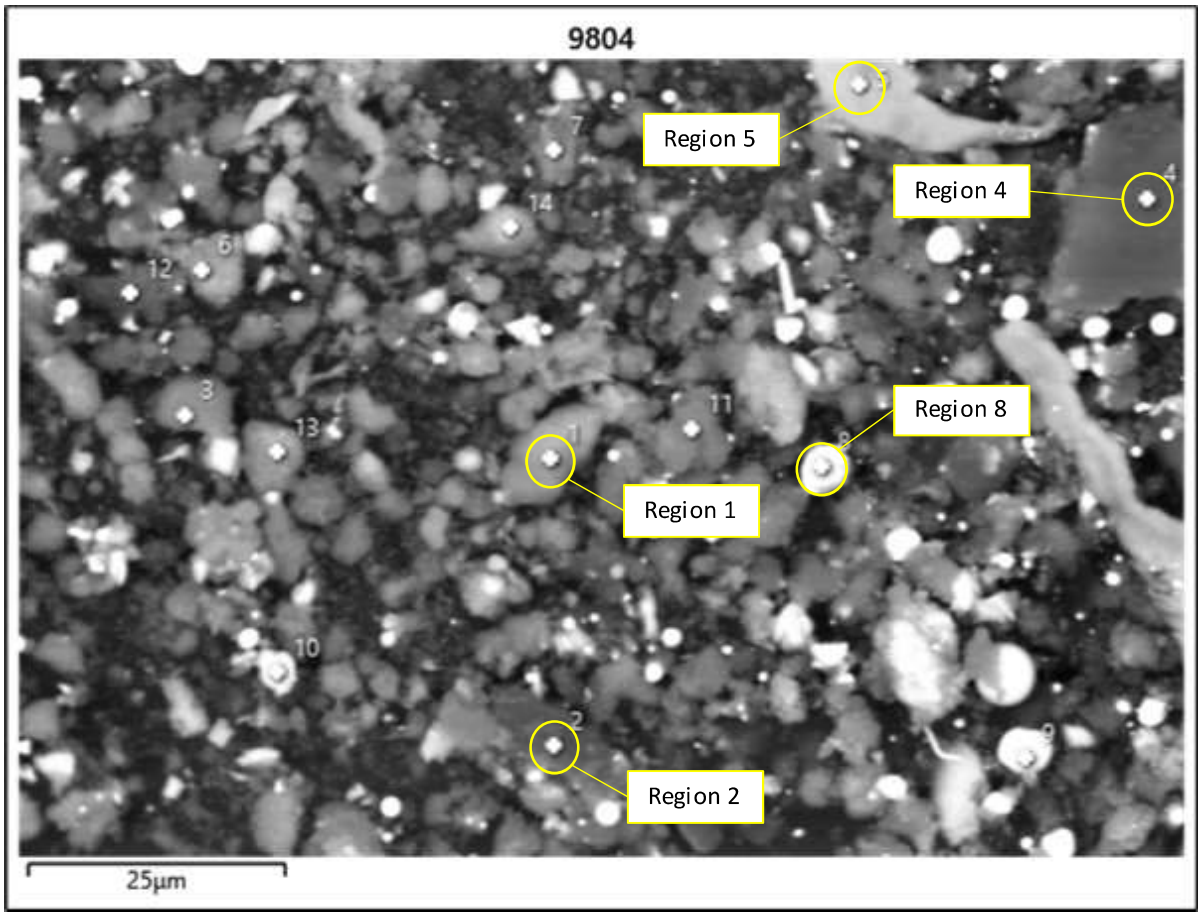

Figure 3-18. High-Magnification SEM Image of EXT-040-Inside Solids.

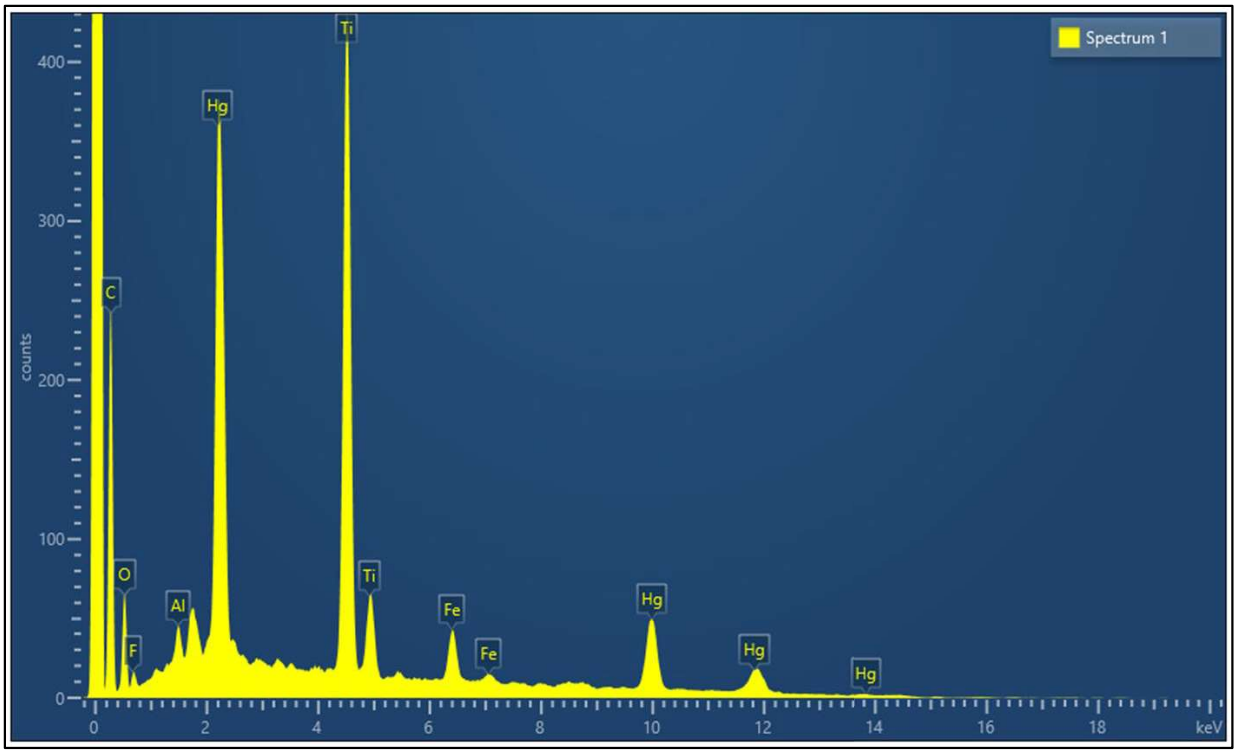

Figure 3-19. EDS Spectrum of Region 1 in High-Magnification EXT-040-Inside Solids SEM Image.

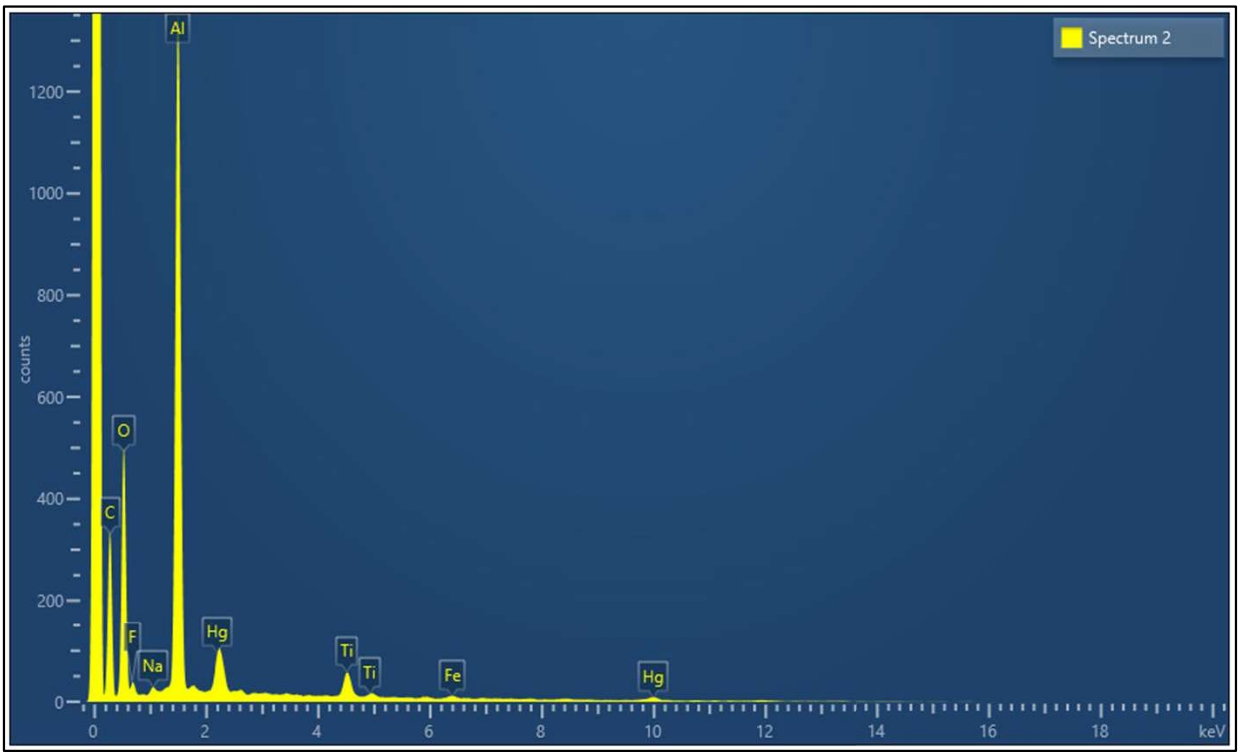

Figure 3-20. EDS Spectrum of Region 2 in High-Magnification EXT-040-Inside Solids SEM Image.

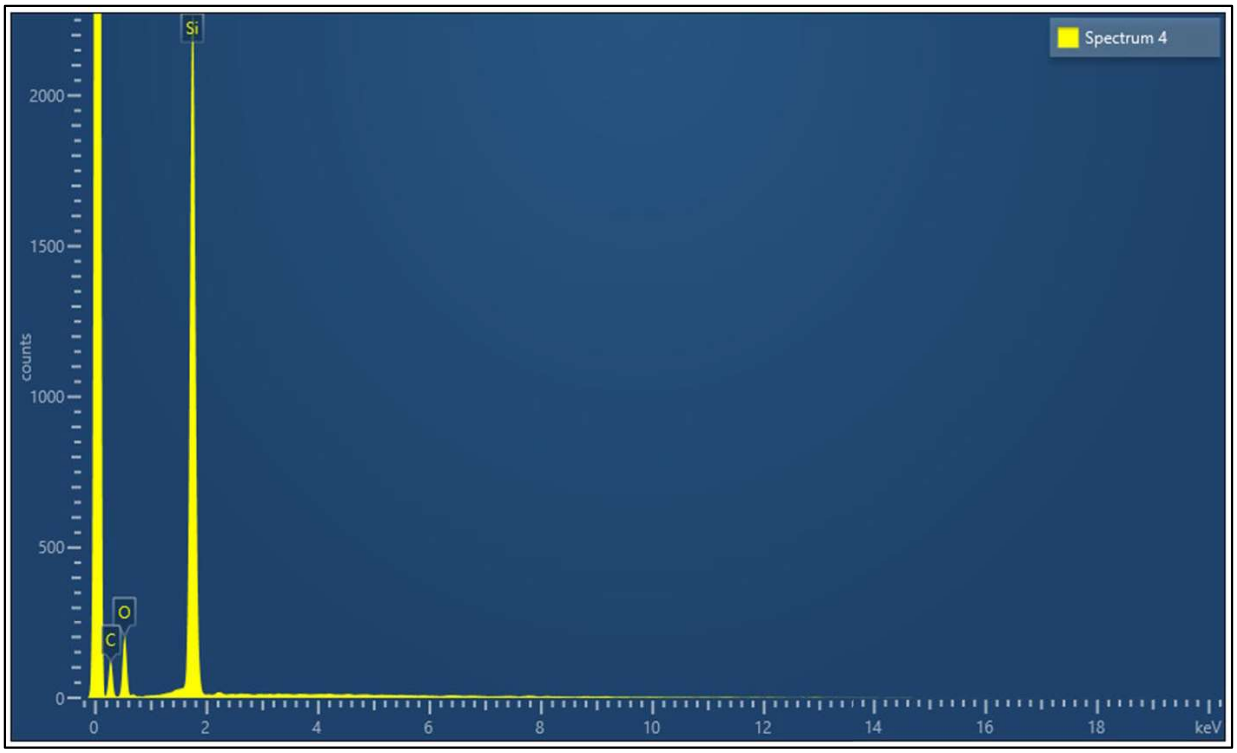

Figure 3-21. EDS Spectrum of Region 4 in High-Magnification EXT-040-Inside Solids SEM Image.

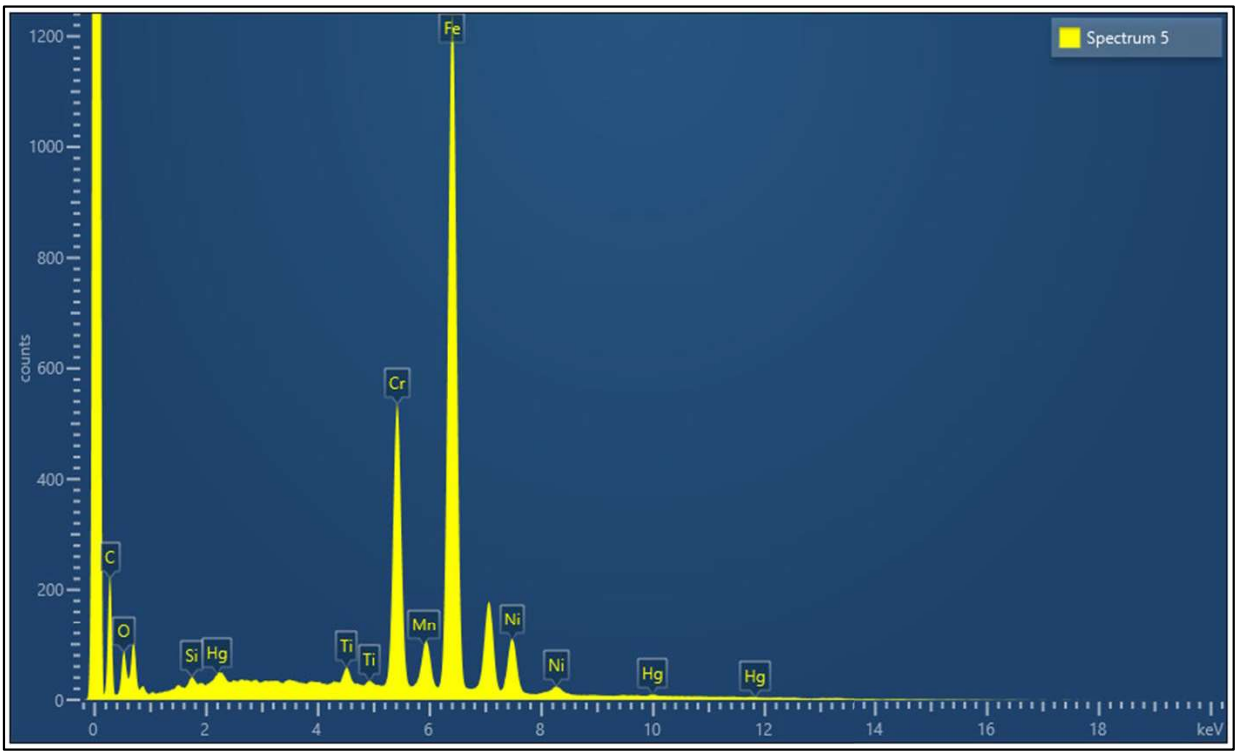

Figure 3-22. EDS Spectrum of Region 5 in High-Magnification EXT-040-Inside Solids SEM Image.

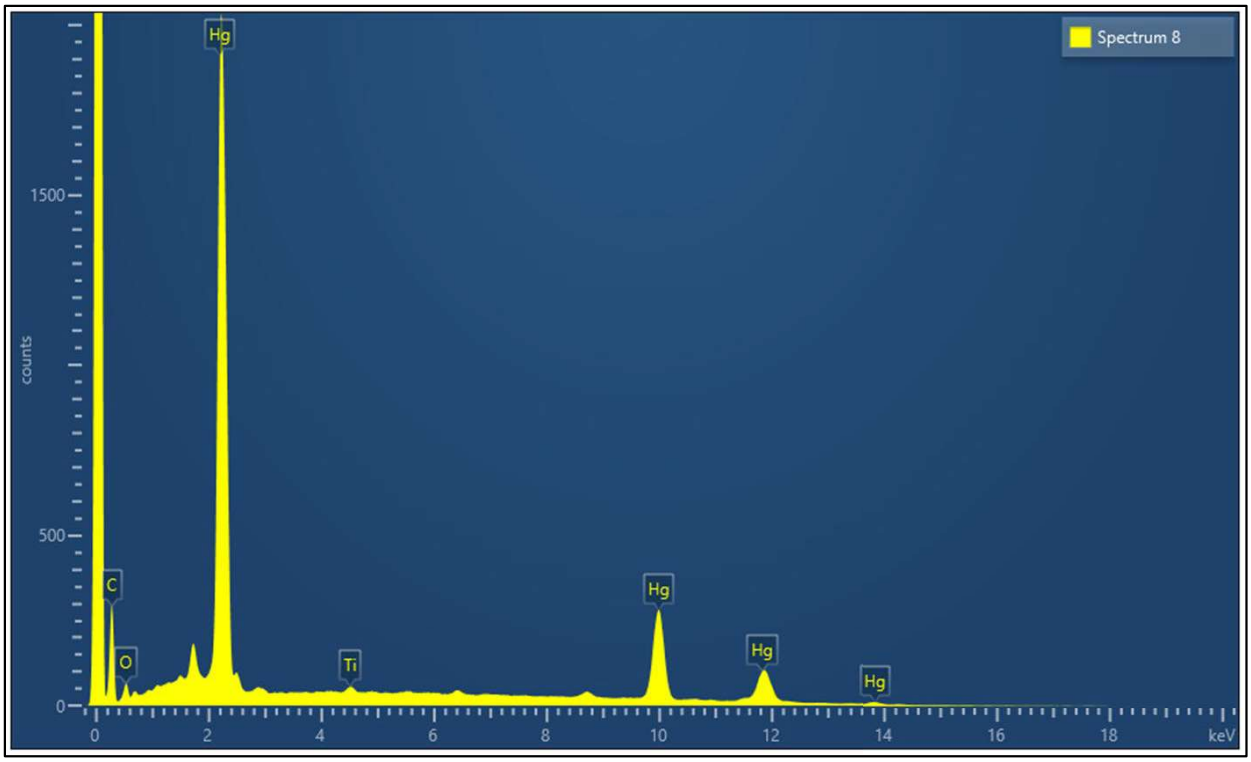

Figure 3-23. EDS Spectrum of Region 8 in High-Magnification EXT-040-Inside Solids SEM Image.

The EDS spectrum for region 1 (Figure 3-19) yields large peaks for titanium and mercury, suggesting co-location of these two elements within the particle shown in region 1. The EDS spectrum of region 2 (Figure 3-20) yields a large peak for aluminum, which may be further evidence of an aluminum-based solid (such as Gibbsite). Curiously, the EDS spectrum for region 4 (Figure 3-21, represented in Figure 3-18 as a relatively large particle) only presents a significant peak for silicon, which may indicate the presence of large silica particles. At this time, it is not clear if this particle is from the SWPF process or from cross-contamination with atmospheric dust. However, it should be acknowledged that the concentration of silicon observed in EXT-040-Inside solids (reported in Table 3-2) does not preclude the possibility of silicon-containing solids. The EDS spectrum for region 5 (Figure 3-22, represented in Figure 3-18 as a relatively large particle) yielded large peaks for co-located iron, chromium, nickel, and manganese. The appearance of these elements as well as the size and shape of the particle observed in Figure 3-18 is consistent with shavings from a ferrous alloy. This is consistent with the expected wear of rotating steel components within the SWPF. Finally, the spherical particle in region 8 yields an EDS spectrum (Figure 3-23) that is consistent with elemental mercury (i.e., most dominant peaks are attributable to Hg, with an apparent Hg:O ratio greatly exceeding that expected from mercury oxide), which may indicate the presence of mercury metal in these solids.

3.3 Analysis of 202-A/B (Scrub Contactors) Solids

3.3.1 Elemental Analysis of 202-A/B Solids

The elemental analysis of 202-A/B solids is given in Table 3-3. The second column reports data obtained from samples digested via aqua regia. The third column reports data obtained from samples digested via special preparation of nitric-sulfuric acids (for Hg) and peroxide fusion (other metals). The fourth column presents the "best value" for each element. The methodology for determining the best value in Table 3-3 is the same as that employed in Table 3-2 in Section 3.2.

Table 3-3. Elemental Analysis of 202-A/B Solids.

Element	Concentration (Aqua Regia) (mg kg^{-1})	Concentration (Peroxide Fusion/Special Prep.) (mg kg^{-1})	Best Value (mg kg^{-1})
Ag	< 9.50	< 776	< 9.50
Al	1,020	3,460	3,460
B	< 21.2	< 62.5	< 21.2
Ba	13.3	< 58.8	13.3
Be	< 0.206	< 5.03	< 0.206
Ca	813	NR†	813
Cd	3.96	< 10.1	3.96
Ce	< 17.7	< 942	< 17.7
Co	1,210	1,670	1,670
Cr	744	1,150	1,150
Cu	24.3	< 157	24.3
Fe	3,160	4,760	4,760
Gd	< 1.22	< 29.9	< 1.22
Hg	415,000	466,000‡	440,500
K	< 225	< 2,900	< 225
La	< 0.668	< 13.9	< 0.668
Li	< 62.8	< 387	< 62.8
Mg	178	116	178
Mn	44.6	76.1	76.1
Mo	71.2	170	170
Na	2,700	NR†	2,700
Ni	117	189	189
P	70.2	< 386	70.2
Pb	74.8	< 241	74.8
S	556	< 965	556
Sb	< 34.4	< 273	< 34.4
Si	250	< 1,250	< 1,250
Sn	< 18.0	< 440	< 18.0
Sr	3.88	< 26.3	3.88
Th	< 24.6	< 600	< 24.6
Ti	16,700	36,400	36,400
U	315	< 293	315
V	< 11.9	< 89.9	< 11.9
Zn	52.6	< 117	52.6
Zr	18.1	NR†	18.1

†The peroxide fusion technique involves the use of sodium peroxide in a zirconium crucible. For this reason, Na and Zr measurements by peroxide fusion are unreliable and are therefore not reported. Additionally, a calcium impurity was observed in the blank sample, suggesting that calcium observed in the peroxide fusion sample may be a result of trace impurities in sodium peroxide. Therefore, Ca is not reported via peroxide fusion.
‡The mercury value reported in the third column is taken from the special preparation using nitric and sulfuric acids. The temperatures employed in peroxide fusion are prohibitive for effective Hg analysis.

The data in Table 3-3 resemble those data seen in Table 3-2, in that mercury is present in abundance (>40%). Similarly, the titanium concentration is significant, reaching as high as 36,400 ppm with peroxide fusion treatment. Other metals (Fe, Al, Cr, etc.) remain observable, but lower than was seen in Table 3-2.

3.3.2 X-Ray Diffraction Analysis of 202-A/B Solids

An XRD spectrum and analysis of 202-A/B solids is given in Figure 3-24. An alternative spectral analysis is given in Figure 3-25.

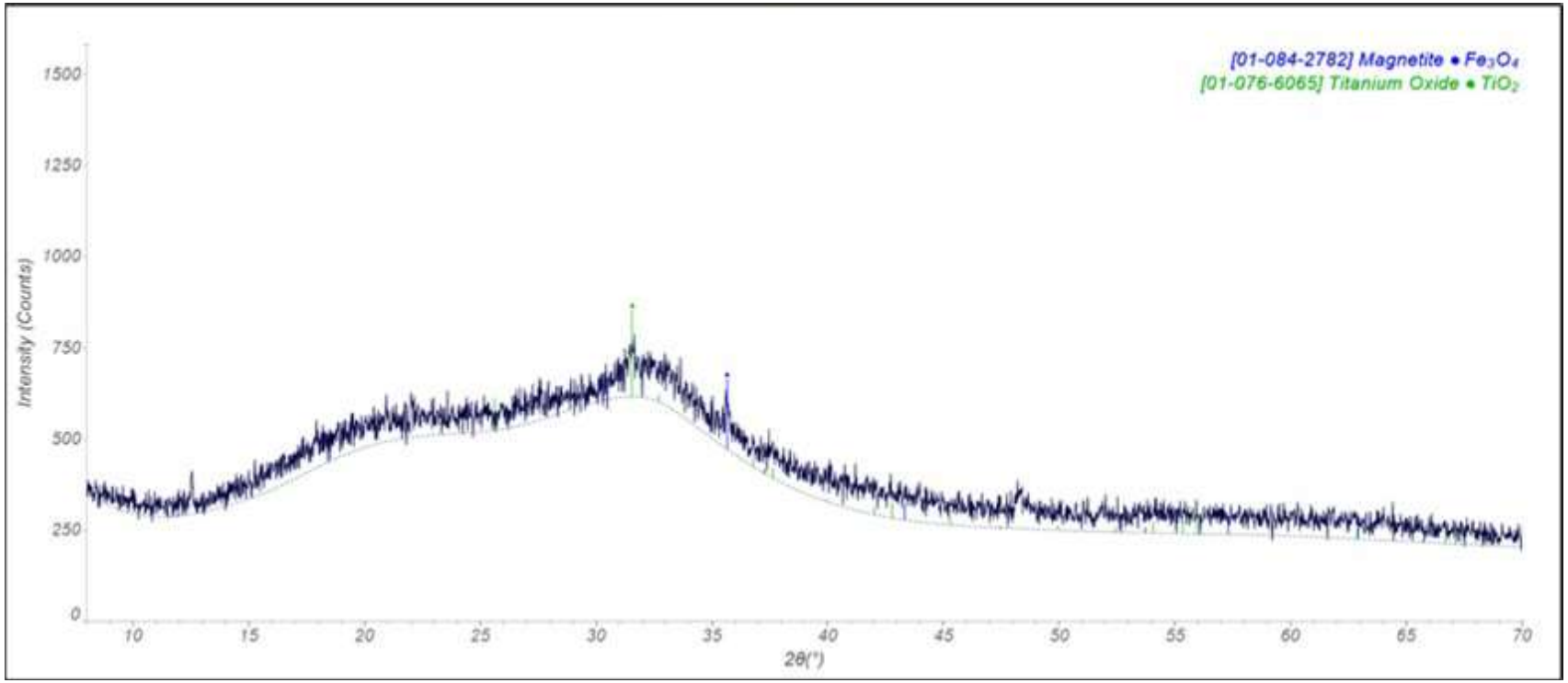

Figure 3-24. XRD Analysis of 202-A/B Solids.

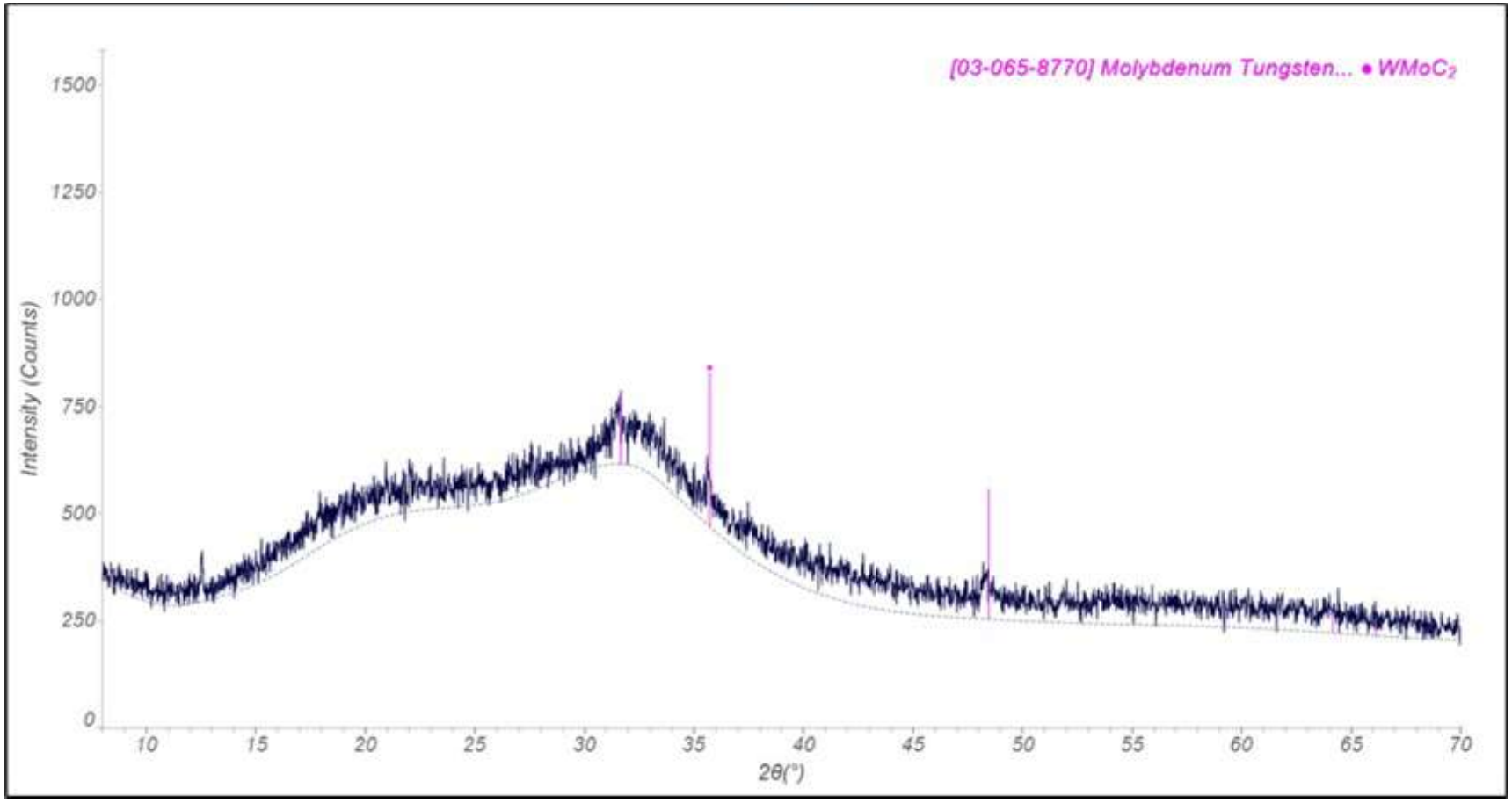

Figure 3-25. Alternative XRD Analysis of 202-A/B Solids.

The XRD spectra in Figure 3-24 and Figure 3-25 indicate that 202-A/B solids are largely amorphous. The analysis offered in Figure 3-24 suggests the presence of Fe_3O_4 and TiO_2. However, the reappearance of an unassigned peak at 48° might indicate the presence of molybdenum tungsten carbide ($MoWC_2$), rather than Fe_3O_4 and TiO_2. The presence of Mo, Fe, and Ti in Table 3-3 combined with the appearance of tungsten in previous SWPF solids samples suggest that either scenario is a possibility. Therefore, the only conclusion that can be confidently given is that 202-A/B solids exhibit little to no degree of crystallinity aside from trace metals.

3.3.3 Scanning Electron Microscopic Analysis of 202-A/B Solids

3.3.3.1 Large Area Scan

A large area SEM image of 202-A/B solids is given in Figure 3-26. An EDS spectrum for the region outlined in white is provided in Figure 3-27. The scale used for reference in the image is 1 mm.

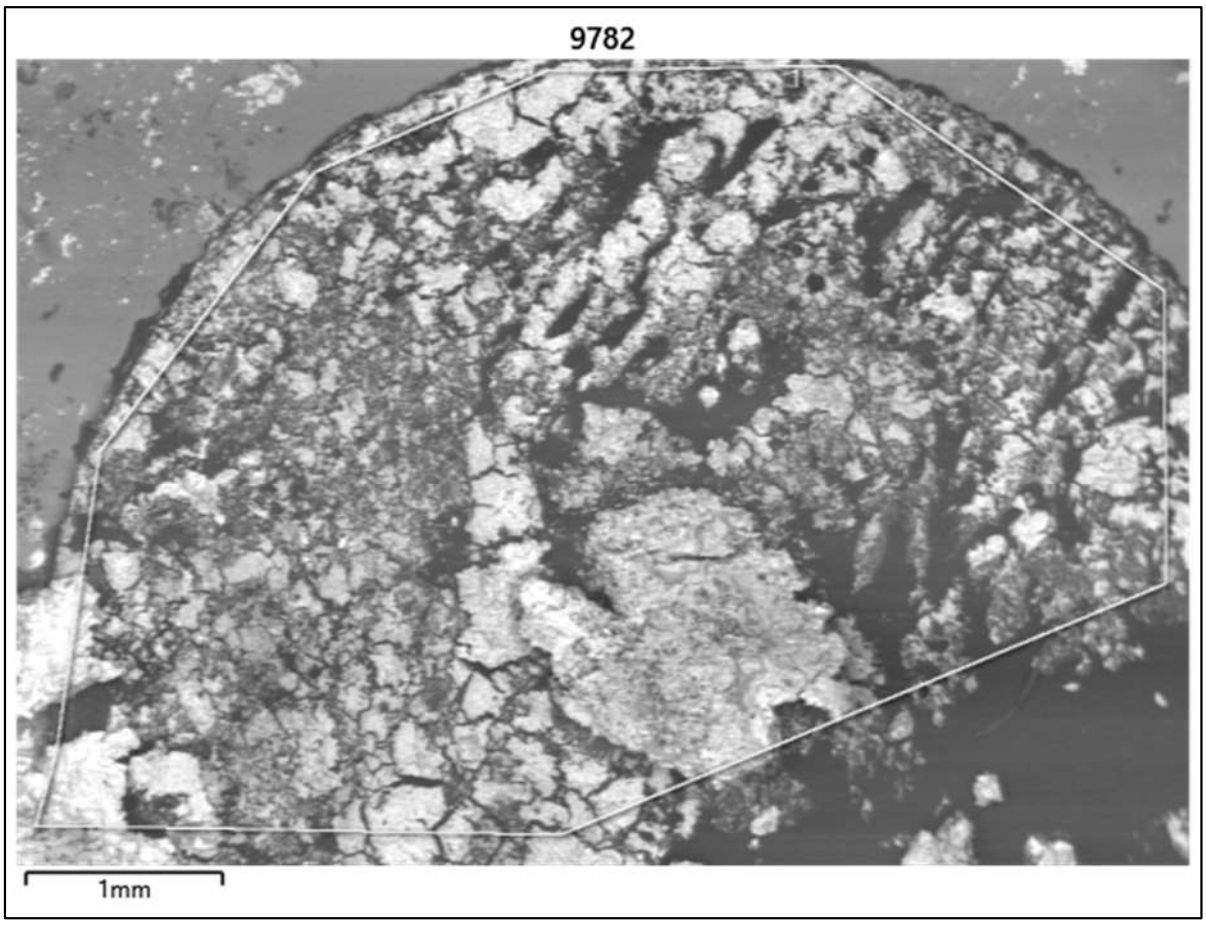

Figure 3-26. Large Area SEM Image of 202-A/B Solids.

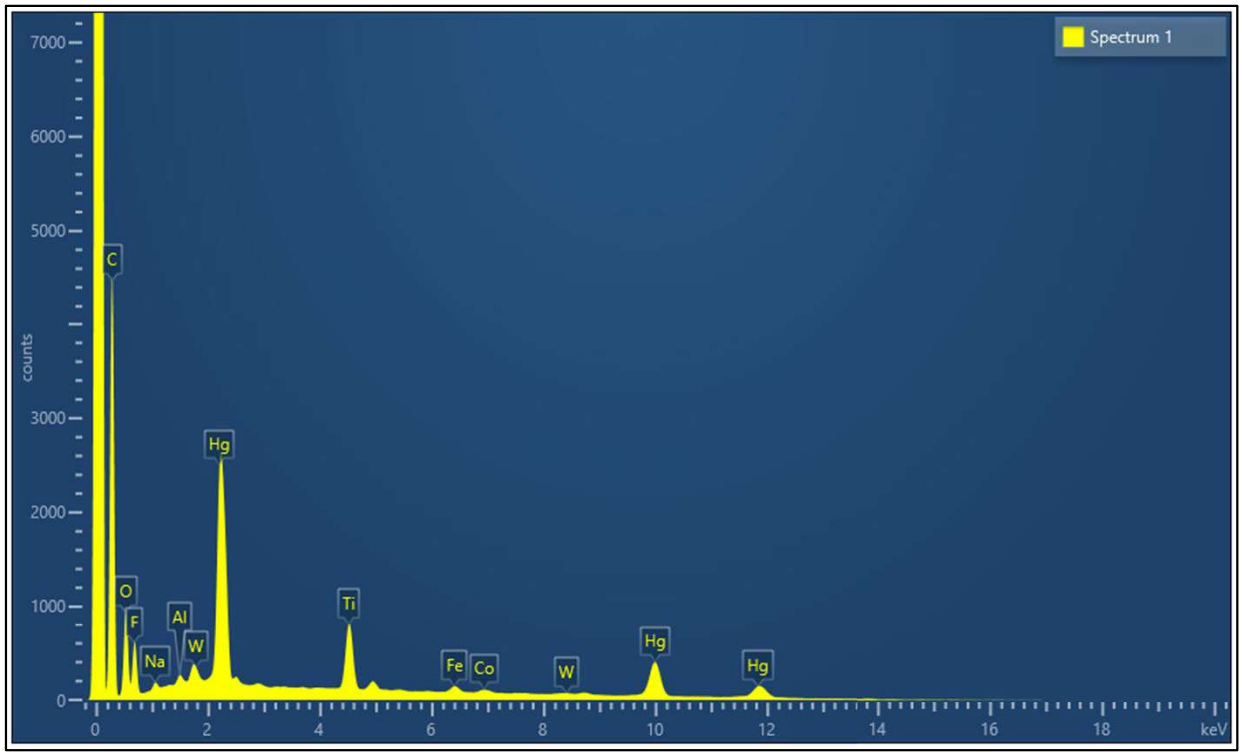

Figure 3-27. Large Area EDS Scan of 202-A/B Solids.

The large area EDS scan for 202-A/B solids in Figure 3-27 shows that several metals are present within these solids. The observed metals include Na, Al, W, Hg, Ti, Fe, and Co, all of which are consistent with EDS spectra taken from previous SWPF solids samples. The presence of fluorine is repeated here, which is consistent with the observation of fluorine in EXT-040-Inside solids (as shown in Figure 3-12). It is unclear if this peak is due to trapped/adsorbed solvent components or if the organic components play an active role in solid formation.

3.3.3.2 Low-Magnification Scan

A low-magnification SEM image of 202-A/B solids is given in Figure 3-28. The scale used for reference in the image is 250 µm. EDS spectra for various regions within the image are given in Figure 3-29, Figure 3-30, Figure 3-31, and Figure 3-32.

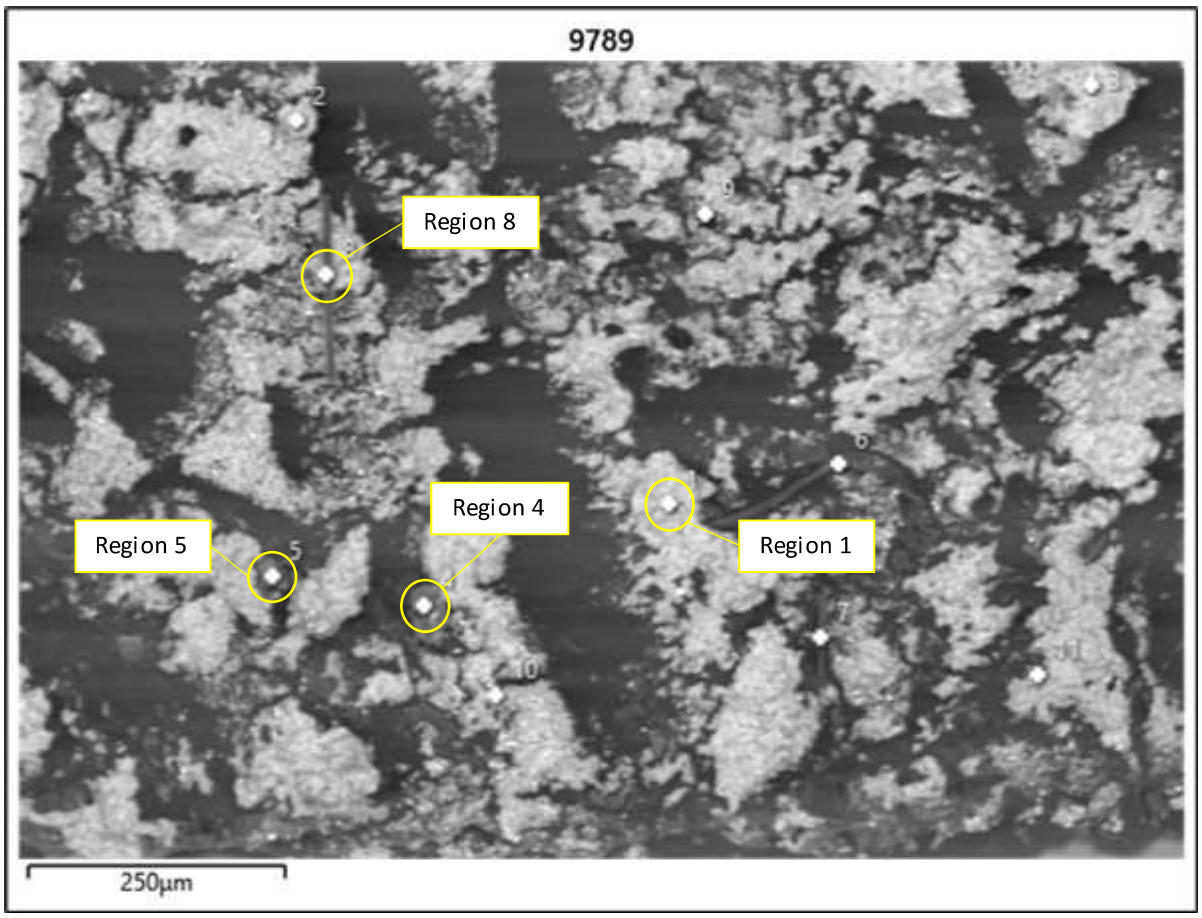

Figure 3-28. Low-Magnification SEM Image of 202-A/B Solids.

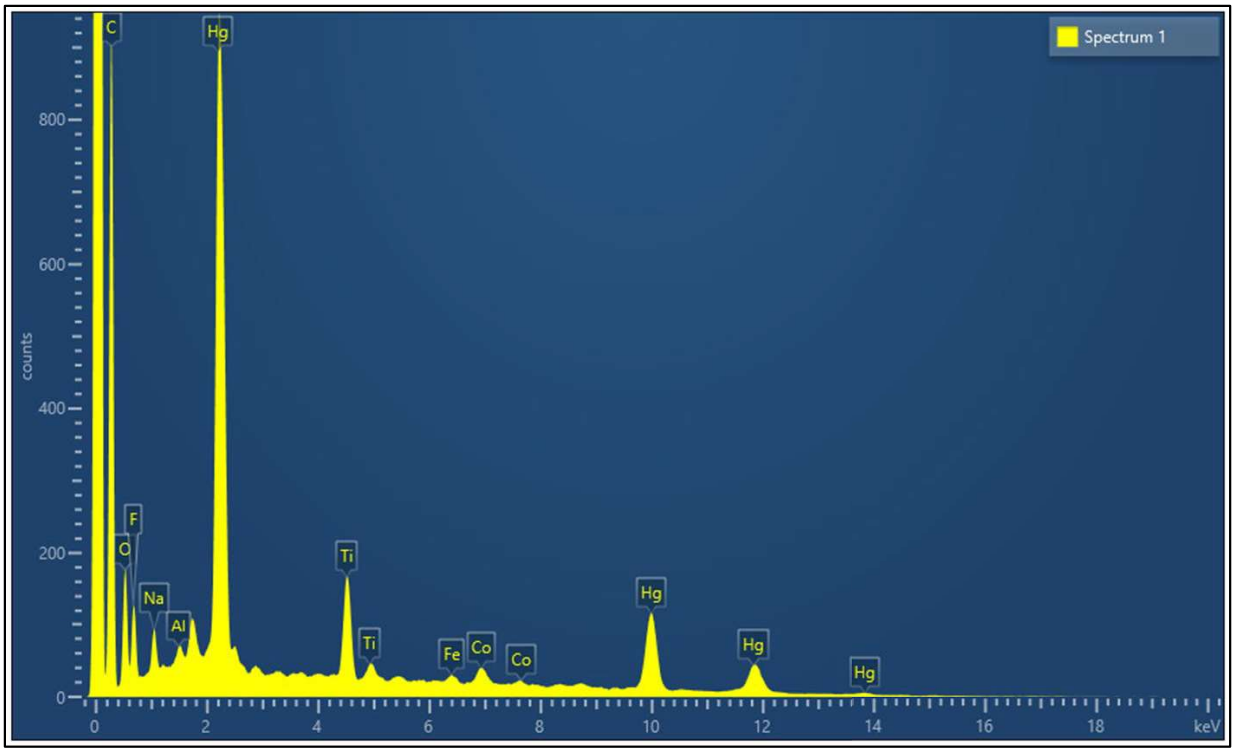

Figure 3-29. EDS Spectrum of Region 1 in Low-Magnification 202-A/B Solids SEM Image.

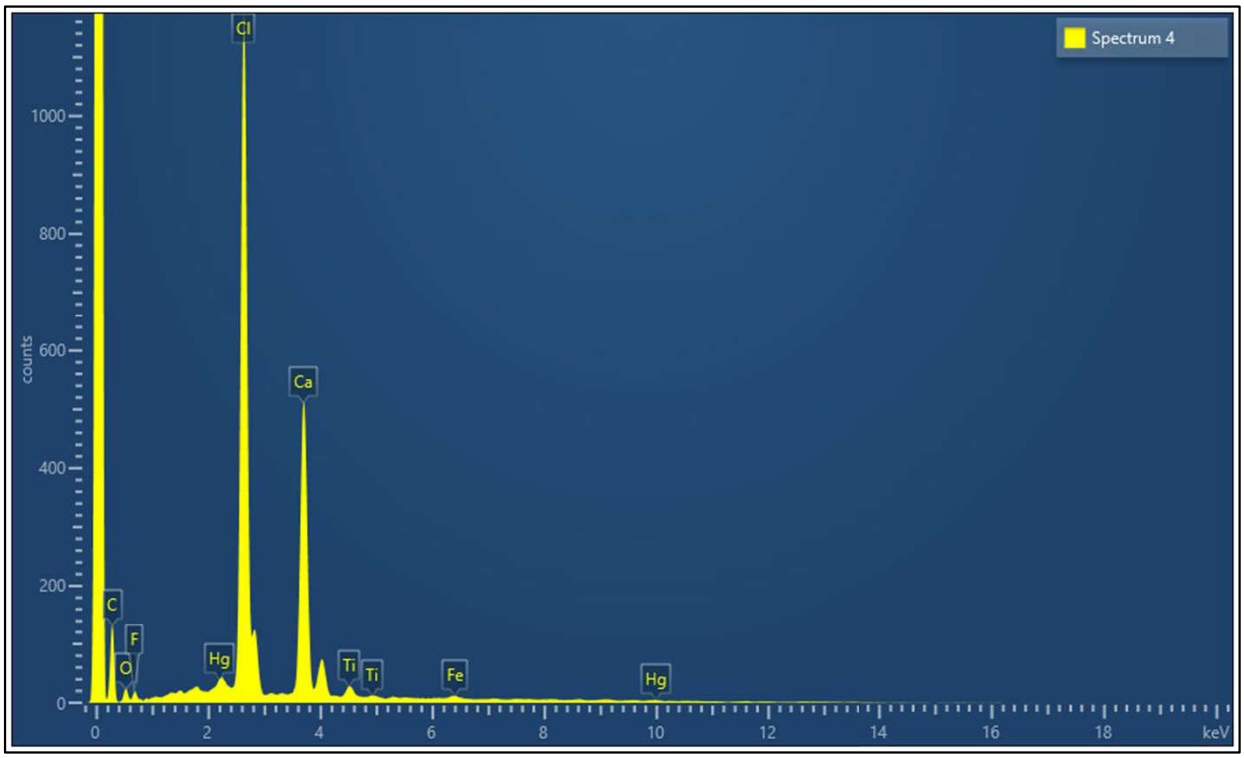

Figure 3-30. EDS Spectrum of Region 4 in Low-Magnification 202-A/B Solids SEM Image.

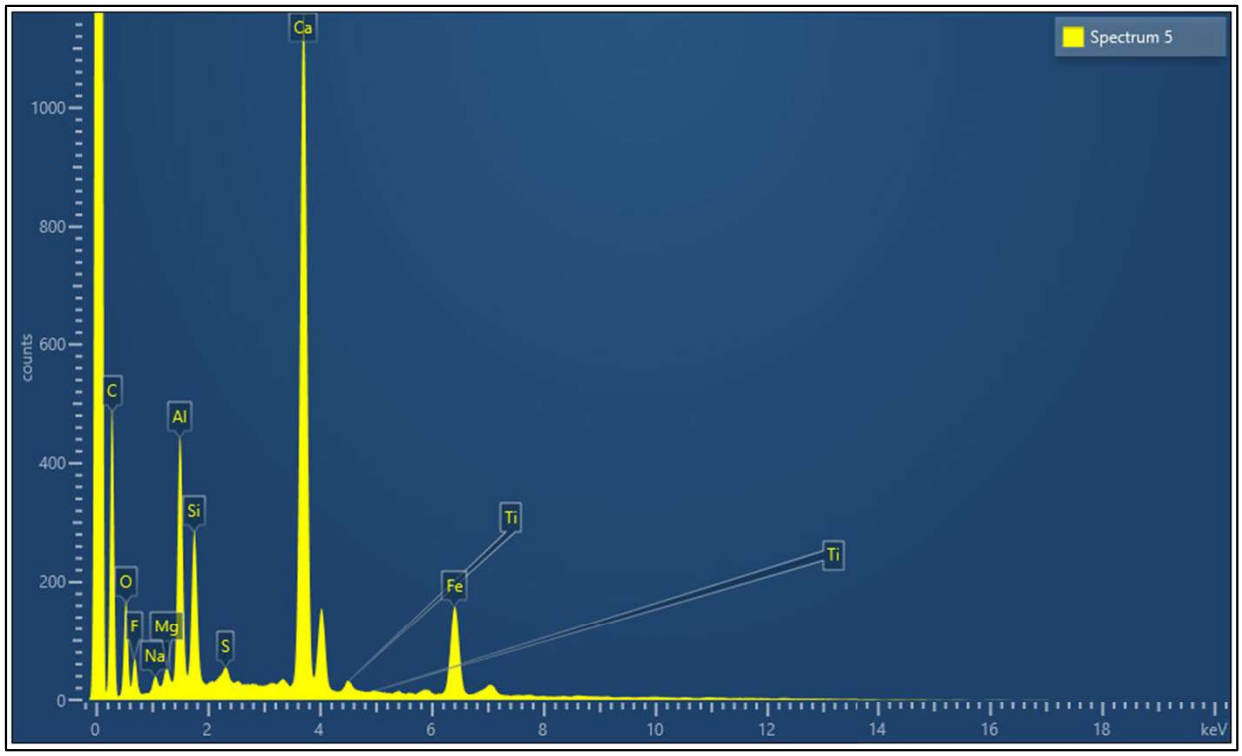

Figure 3-31. EDS Spectrum of Region 5 in Low-Magnification 202-A/B Solids SEM Image.

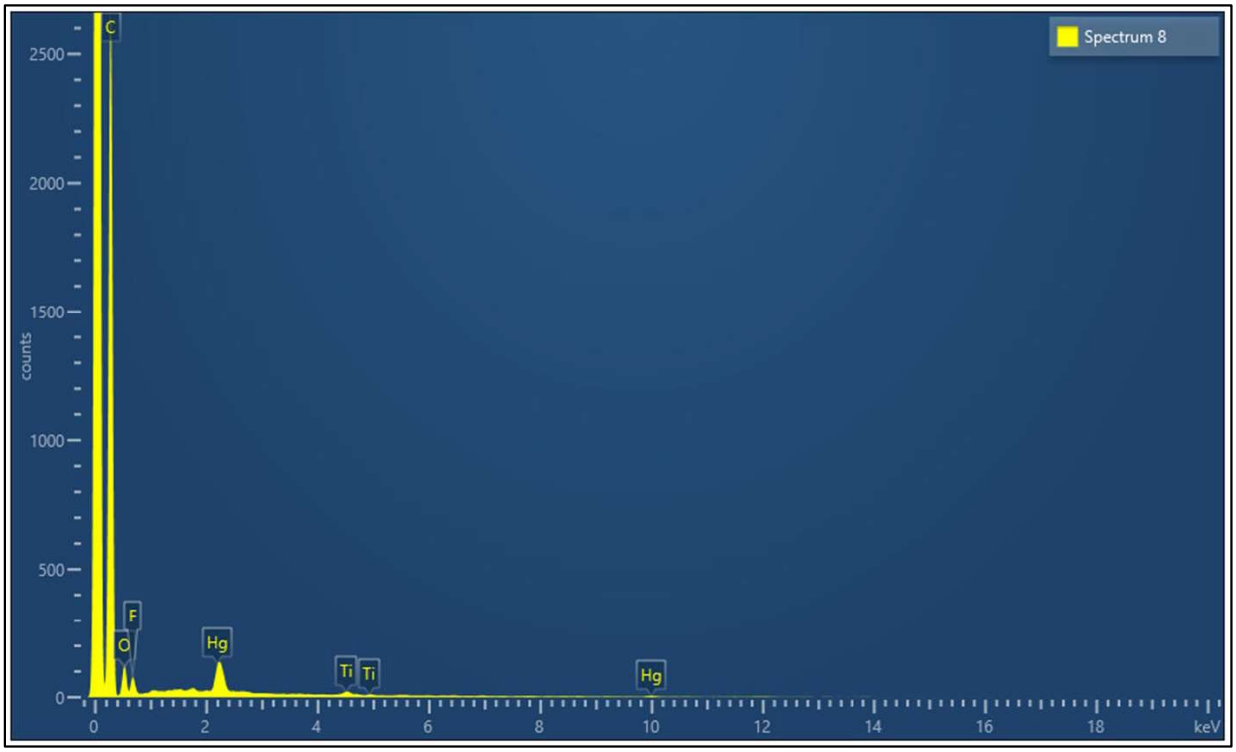

Figure 3-32. EDS Spectrum of Region 8 in Low-Magnification 202-A/B Solids SEM Image.

The EDS spectrum taken from region 1 (Figure 3-29) indicates significant presence of Hg and Ti, with minor contributions from Fe, Co, Na, and Al, while the spectrum taken from region 4 (Figure 3-30) indicate a localized composition rich in Ca and Cl. Figure 3-31 shows that region 5 also contains a significant amount of Ca, but does not appear to contain as much Cl as observed in region 4. At first glance, the EDS spectra for region 8 (Figure 3-32) might suggest a heavy presence of carbon. However, closer inspection of Figure 3-28 reveals that region 8 is taken around what appears to be a large, fibrous particle. It is therefore suspected that the object identified in region 8 is likely a splinter from sample sticks used to obtain the solids samples from contactors 201A and 201B and is not representative of solids within the SWPF. The exact contribution of sample stick cross contamination on elemental mass balance is uncertain but is believed to be low when compared to the uncertainty related to sampling bias involved with handling mixed solids.

3.3.3.3 High-Magnification Scan

A high-magnification SEM image of 202-A/B solids is given in Figure 3-33. The scale used for reference in the image is 25 µm. EDS spectra for various regions within the image are given in Figure 3-34, Figure 3-35, and Figure 3-36.

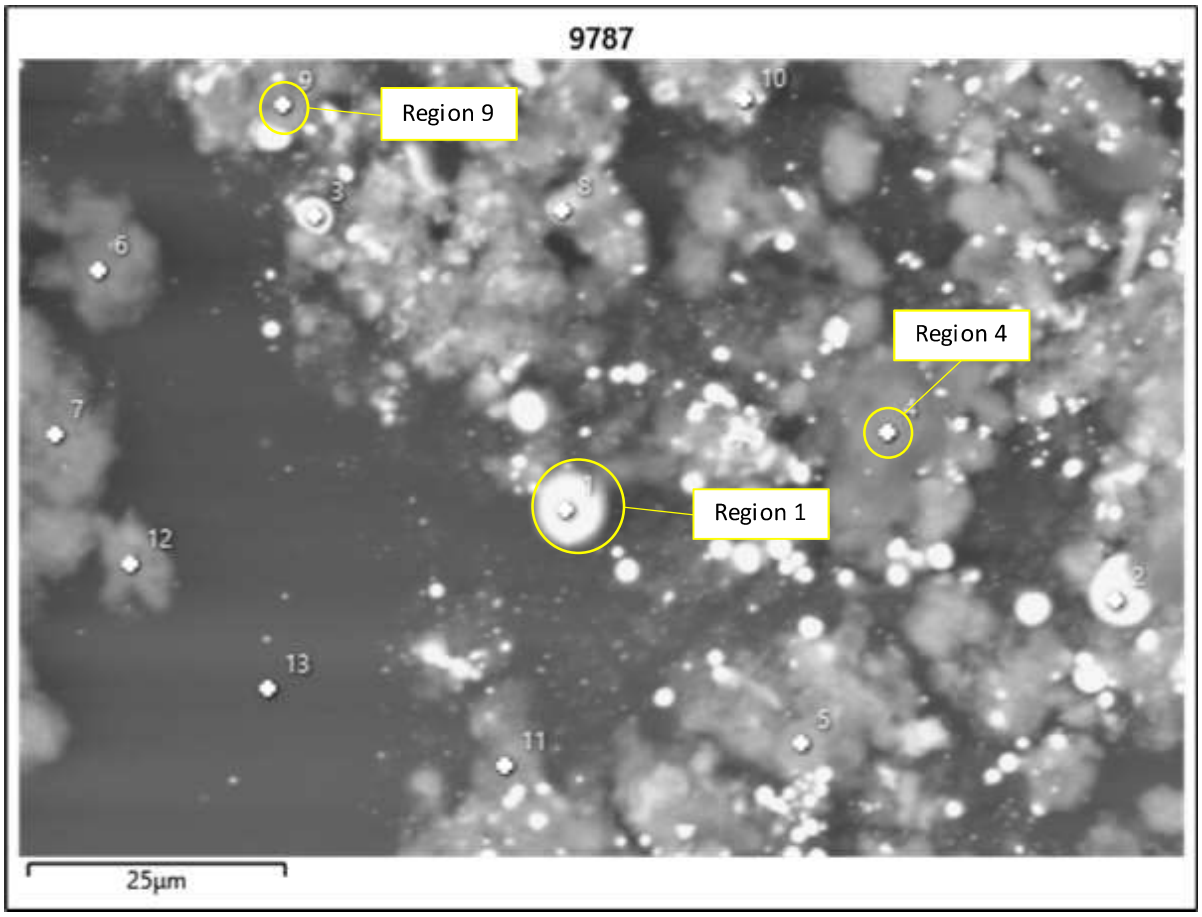

Figure 3-33. High-Magnification SEM Image of 202-A/B Solids.

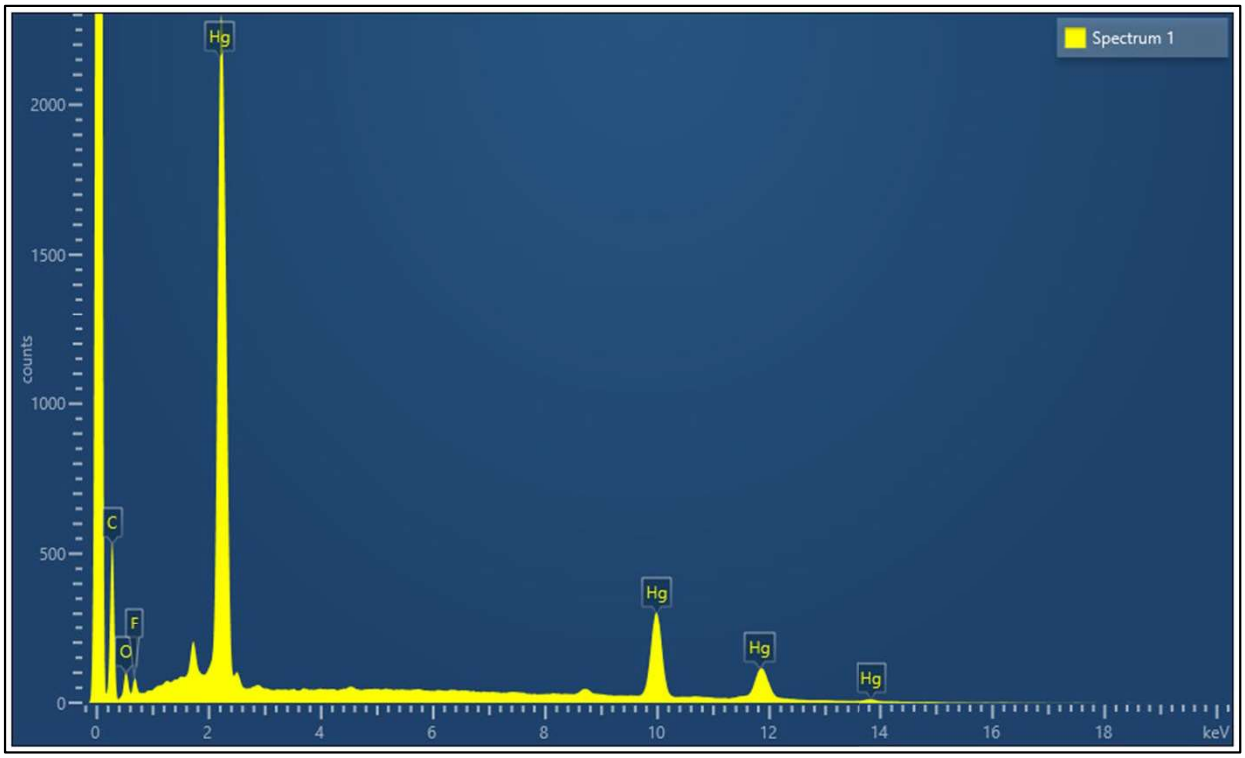

Figure 3-34. EDS Spectrum of Region 1 in High-Magnification 202-A/B Solids SEM Image.

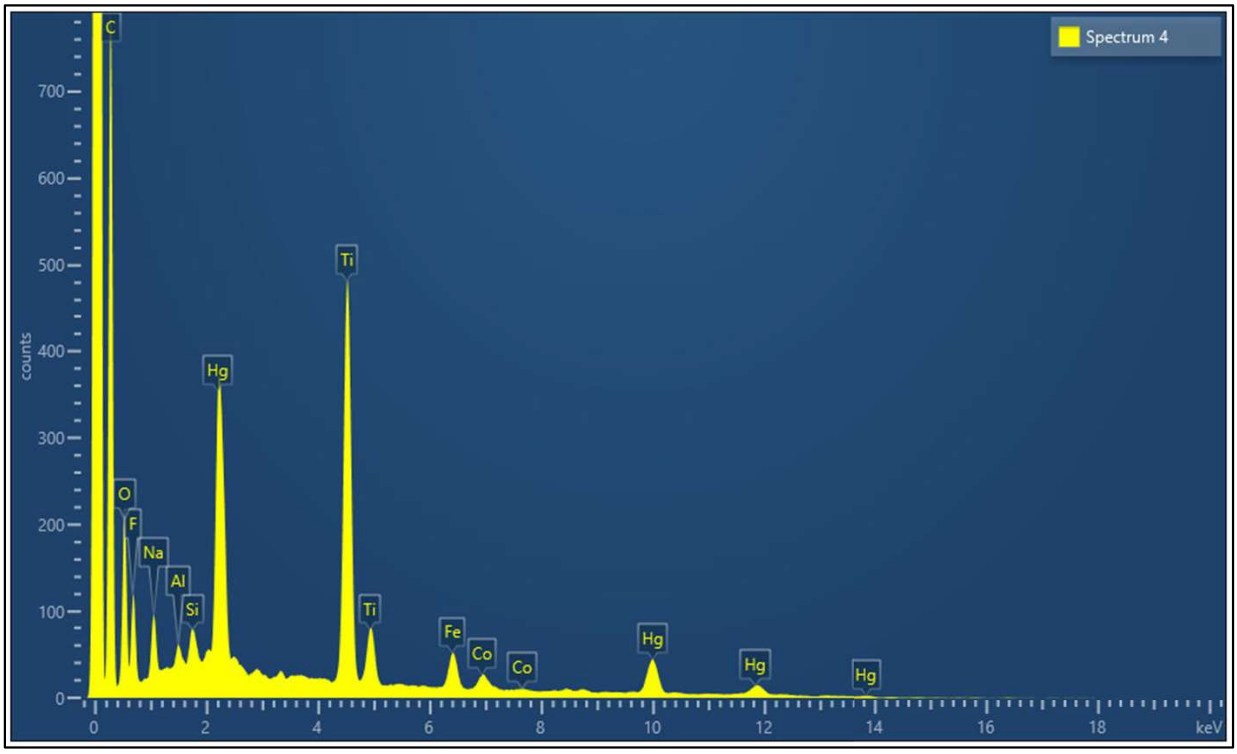

Figure 3-35. EDS Spectrum of Region 4 in High-Magnification 202-A/B Solids SEM Image.

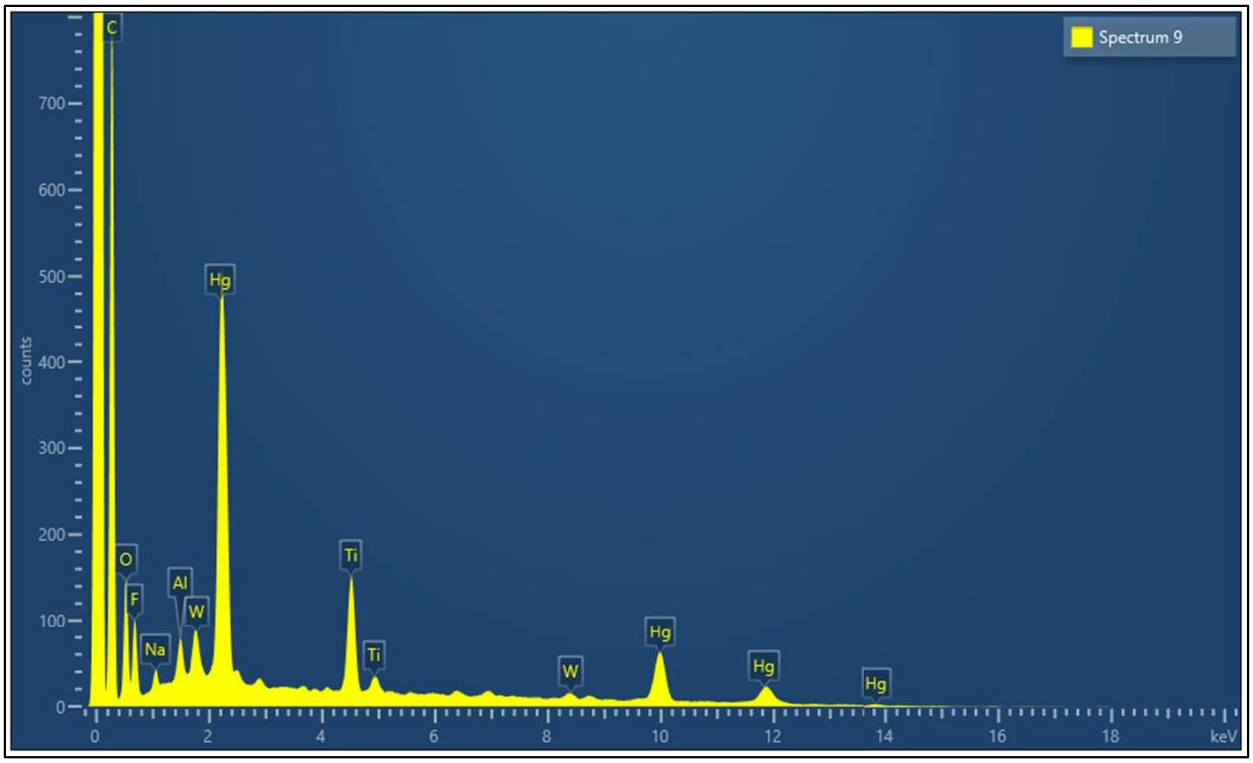

Figure 3-36. EDS Spectrum of Region 9 in High-Magnification 202-A/B Solids SEM Image.

Upon first inspection of Figure 3-33, it is immediately clear that large, spherical particles of various size are pervasive throughout the solids sample. The EDS spectrum of region 1 (Figure 3-34) reveals that these particles mostly consist of Hg. The peak height of Hg compared to that of O, while not quantitative, does indicate that at least some of the Hg present within these spherical particles is elemental Hg. The EDS spectrum of region 4 (Figure 3-35) indicates the presence of co-located Ti and Hg. The nature of this co-location (i.e., co-precipitation, entrainment, etc.) is unknown at this time. Similar co-location behavior is observed in the EDS spectrum from region 9 (Figure 3-36).

3.4 Solids Categorization

It is helpful to compare the results obtained from SWPF contactor solids samples to those obtained from previous SWPF samples in order to categorize the solids present. Table 3-4 shows the concentrations of major elements identified in contactor solids samples as well as concentrations observed in previous SWPF solids samples.[8]

Table 3-4. Concentrations of Major Elements in SWPF Solids (in mg kg^{-1}).

Element	Contactors 202-A/B	EXT-040-Inside	August 2022 DSSC Solids	December 2021 DSSC Solids	April 2022 Tank 202 Emulsion Layer	March 2022 Tank 202 "As Received" Sample
Al	3,460	7,280	1,020	3,070	10.8	2,310
Ba	13.3	33.5	17.4	15.8	1.04	204
Ca	813	740	279	69.6	18.2	3,370
Cd	3.96	8.03	6.82	5.41	0.188	34
Co	1,670	1,220	278	337	10.4	1,910
Cr	1,150	4,910	275	306	16.1	3,850
Cu	24.3	74.4	< 13.7	< 11.6	1.59	321
Fe	4,760	21,500	1,380	2070	112	24,800
Hg	440,500	681,000	2,500	44,400	1,600	142,000
Mg	178	285	108	62.8	6.65	1210
Mn	76.1	402	22.7	26.2	2.65	670
Mo	170	235	9.91	15.4	0.636	76.7
Na	2,700	7,620	20,600	1,790	549	37,400
Ni	189	2,020	115	106	9.07	2,180
Pb	74.8	77	< 33.3	< 28.9	0.809	160
Si	< 1,250	5,520	81.5	105	20.1	728
Sr	3.88	6.19	< 2.39	< 2.31	1.55	334
Ti	36,400	50,300	8,110	18,300	562	71,200
U	315	164	136	203	< 1.46	< 266
Zn	52.6	50.8	25.3	27.9	0.838	138
Zr	18.1	12.4	< 7.77	14.3	0.422	51.2

The data in Table 3-4 can be used to assess correlation between pairs of elements in SWPF solids. Correlation is useful because it may indicate the presence of unique solids that can be traced to single unit operations within the SWPF. An assessment of the Pearson correlation coefficient of each element combination is offered in Figure 3-37 for all of the samples listed above. In the correlation assessment shown, higher-magnitude positive values indicate a greater degree of direct correlation (elevated concentration of one compound occurs with elevated concentration of another compound), while higher-magnitude negative values indicate a greater degree of inverse correlation (elevated concentration of one compound occurs with decreased concentration of another compound). Values near zero indicate little to no sign of correlation. In Figure 3-37, correlation values greater than 0.95 are highlighted in green for ease of identification.

Al	Al																			
Ba	0.013	Ba																		
Ca	0.086	0.977	Ca																	
Cd	0.048	0.994	0.967	Cd																
Co	0.484	0.662	0.793	0.660	Co															
Cr	0.749	0.586	0.632	0.595	0.707	Cr														
Cu	-0.006	0.998	0.983	0.999	0.639	0.580	Cu													
Fe	0.589	0.774	0.799	0.778	0.752	0.966	0.798	Fe												
Hg	0.905	-0.036	0.106	-0.028	0.594	0.718	-0.196	0.544	Hg											
Mg	0.088	0.993	0.993	0.987	0.737	0.647	0.997	0.818	0.067	Mg										
Mn	0.408	0.893	0.903	0.891	0.752	0.886	0.924	0.975	0.367	0.922	Mn									
Mo	0.883	0.055	0.206	0.064	0.682	0.747	-0.100	0.593	0.993	0.161	0.433	Mo								
Na	-0.132	0.879	0.842	0.908	0.475	0.439	0.999	0.614	-0.178	0.865	0.736	-0.089	Na							
Ni	0.587	0.749	0.760	0.754	0.685	0.969	0.766	0.995	0.527	0.789	0.964	0.569	0.606	Ni						
Pb	0.284	0.892	0.946	0.919	0.901	0.683	0.906	0.833	0.156	0.928	0.896	0.268	0.897	0.772	Pb					
Si	0.923	-0.018	0.059	-0.001	0.442	0.808	-0.185	0.630	0.996	0.065	0.442	0.982	-0.112	0.665	0.094	Si				
Sr	-0.198	0.992	0.972	0.980	0.565	0.410	0.981	0.665	-0.371	0.979	0.833	-0.273	0.987	0.629	0.844	-0.383	Sr			
Ti	0.567	0.800	0.865	0.806	0.921	0.874	0.824	0.933	0.551	0.854	0.929	0.625	0.595	0.893	0.967	0.492	0.717	Ti		
U	0.021	-0.511	0.480	-0.874	0.718	-0.175	-1.000	-0.198	0.271	0.028	-0.221	0.322	-0.696	-0.310	-1.000	-0.091	-1.000	0.317	U	
Zn	0.230	0.948	0.980	0.952	0.856	0.681	0.950	0.828	0.211	0.971	0.907	0.309	0.805	0.782	0.990	0.143	0.911	0.924	0.577	Zn
Zr	0.020	0.954	0.964	0.965	0.773	0.512	0.955	0.709	-0.042	0.959	0.827	0.070	0.946	0.655	0.963	-0.101	0.943	0.853	0.997	0.981

Figure 3-37. Correlation Coefficients for Each Element Pair Based on Concentrations from SWPF Solids Samples.

The data from the correlation assessment given in Figure 3-37 can be combined with observations from sample analyses made in Sections 3.1, 3.2, and 3.3 to categorize the types of solids observed. This categorization is given in Table 3-5.

Table 3-5. Categorization of Solids/Elements Observed in SWPF Solids.

Solids Grouping	Contributing Elements	Characteristics
Hg-Related Solids	Hg, Mo, Si, Ti	• Presence of elemental Hg confirmed via SEM-EDS • Concentrations of Hg, Mo, Si closely correlated throughout SWPF solids samples • Hg, Ti appear co-located in several EDS spectra
Ferrous Alloy Solids	Fe, Mn, Cr, Ni	• Signature peaks for Fe, Mn, Cr, Ni appear at consistent ratios in EDS spectra • Ratios of Fe, Mn, Cr, and Ni concentrations measured via ICP-ES appear consistent
Alkali/Alkaline Earth-containing Solids	Ba, Ca, Cd, Cu, Mg, Na Pb, Sr, Ti, U, Zn, Zr	• Concentrations are closely correlated throughout SWPF solids samples
Hardened Surface Solids	W, Co, Mo	• Tungsten particles confirmed via SEM-EDS • XRD results indicate possible presence of $MoWC_2$ • EDS spectra indicate presence of Co in solids
Aluminum-Based Solids	Al, Si	• Decreased solubility of Al, Si might indicate presence of insoluble aluminum species • XRD results suggest presence of Gibbsite ($Al(OH)_3$) • EDS spectra yield peaks from Al- and Al/Si-rich particles
Salt Solids	Na, K, S, C, O, N	• ICP-AES results indicate high concentration of sodium • XRD results reveal high degree of crystallinity, presence of sodium salts • EDS spectra suggest presence of salt species

The groupings in Table 3-5 suggest that the solids observed in SWPF CSSX processing can divided into at least six categories: 1) Hg-Related Solids, 2) Ferrous Alloy Solids, 3) Alkali/Alkaline Earth-Containing Solids, 4) Hardened Surface Solids, 5) Aluminum-Based Solids, and 6) Salt Solids.

Hg-related solids are the largest contributor to SWPF solids, by mass. Large concentrations of Hg were confirmed by DMA and SEM-EDS analyses. While EDS spectra indicate that Hg is often present as elemental Hg in these solids, ICP-AES results indicate that Mo and Si concentrations are strongly correlated with Hg concentrations. The mechanism of this potential co-location is unclear at this time. While Ti-Hg correlation was not confirmed in ICP-AES concentrations, several EDS spectra suggest that Ti and Hg are often co-located within SWPF solids, which serves as the basis for grouping within Hg-related solids.

Ferrous alloy solids are postulated to be the second-largest contributor to SWPF solids. Recurring ratios of Fe, Ni, Cr, and Mn are confirmed via ICP-AES as well as EDS spectra. The use of these elements in stainless-steel formulations suggests the possibility that these solids come from steel components (e.g., expected wear of rotating equipment) within the SWPF, rather than from chemical precipitation within the CSSX process.

Alkali/Alkaline Earth-containing solids are postulated based on the correlation of several alkali and alkaline earth metals (e.g., Ba, Ca, Na, Mg, Sr). However, beyond a small subset of EDS spectra that identify calcium-rich particles, no physical evidence exists to suggest that these metals are present as distinct solids. Instead, it is possible that these elements are present due to entrainment of CSS material upon precipitation/collection of other solids.

Hardened surface solids are postulated based on the observation of small tungsten particles via SEM-EDS. Additionally, evidence of cobalt was observed in EDS spectra and ICP-AES measurements. Finally, a potential identification of molybdenum tungsten carbide ($MoWC_2$) was made via XRD, which is why Mo is included in the hardened surface solids category as a potential contributor. The presence of tungsten particles visible via SEM suggests that the expected wear of hardened surfaces within the SWPF CSSX process may be the source of these solids rather than a chemical precipitation process.

Aluminum-based solids are postulated based on the appearance of Gibbsite in XRD spectra and aluminum-rich particles in SEM-EDS spectra. Additionally, the increased solubility of aluminum when digested via peroxide fusion (compared to that obtained with aqua regia) is consistent with the presence of insoluble aluminum species. Furthermore, aluminum chemistry has previously been identified as a challenge for CSSX processing at SRS under the operation of the Modular CSSX Unit (MCU).[9] This further supports the notion that some aluminum-based solids are present within SWPF solids.

Salt solids are postulated based on the presence of salt-related elements via ICP-AES (Na, K, S) as well as the appearance of Na_2CO_3, NaOH, and $NaNO_3$ observed via XRD. Additionally, the concentration of Na observed in EXT-007 solids via ICP-AES is consistent with that of undissolved sodium salts, which further suggests that these solids likely formed from evaporated residual salt solution.

3.5 Potential Sources of Solids

3.5.1 Hg-Related Solids

A potential mechanism for Hg precipitation in the SWPF has been identified in the literature. Hg precipitation in the presence of strong base has been observed for both Hg(I) and Hg(II) species.[10] When dissolved in nitric acid, Hg^{2+} precipitates as insoluble HgO (yellow solid) upon treatment with sodium hydroxide. Similarly, Hg^{+} in nitric acid solution precipitates as a blend of microscopic Hg droplets and HgO that appears dark in color when combined with NaOH.

The color of solids recovered from SWPF contactors (dark) as well as the confirmed presence of elemental Hg is consistent with the precipitation mechanism of Hg^{+} in nitric acid upon treatment with hydroxide. This hypothesis is given further support when evaluating the aqueous streams surrounding the contactors where solids have been recovered.

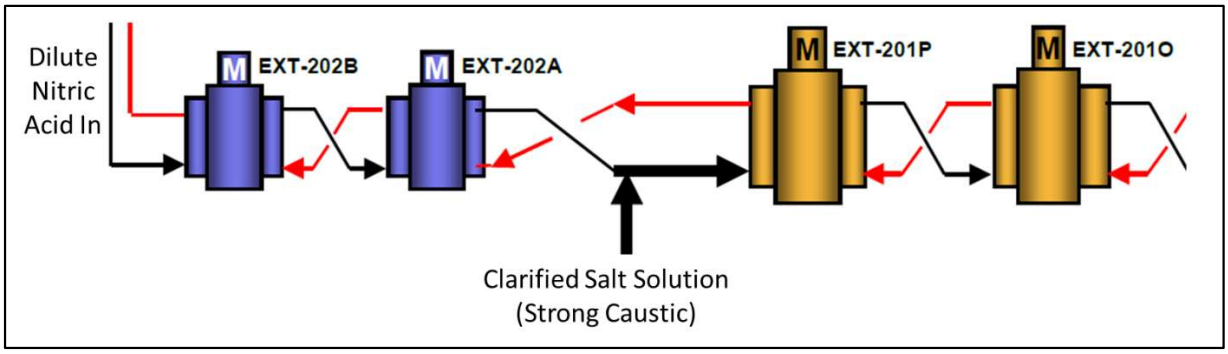

Figure 3-38. Partial Process Flow Diagram of SWPF CSSX Process.

As the partial process flow diagram in Figure 3-38 shows, the four contactors discussed in this report center around a part of the process where dilute nitric acid is combined with strong caustic in the form of Clarified Salt Solution (CSS). At this point in the process, 0.05 M HNO_3 is combined with CSS at the design basis flow rates of 1.4 and 21.6 gal min^{-1}. Simultaneously, approximately 0.2% volume entrainment of CSS-in-solvent is expected to be carried back into EXT-202A from EXT-201P, yielding a dilution of 0.014 gal min^{-1} of CSS into 1.4 gal min^{-1} of 0.05 M HNO_3.[11] Under these operations, pH swings in either direction (low-to-high or high-to-low) can be achieved. Given the presence of insoluble elemental Hg in dark solids and the potential for pH swings in the contactors where the solids were recovered, the Hg^+ precipitation mechanism seems a likely candidate for Hg precipitation. If this mechanism is confirmed to be responsible for Hg precipitation, it would indicate the concentration of Hg such that the equilibrium concentration of product mercury species (i.e., elemental Hg) is higher than the solubility of the product mercury species, resulting in precipitation.

Several EDS spectra of contactor solids indicate that Hg and Ti are often co-located (see Figure 3-17, Figure 3-19, Figure 3-29, Figure 3-35, and Figure 3-36) within solids recovered from SWPF contactors. Potential mechanisms for the co-location of Hg and Ti include co-precipitation, entrainment, and amalgamation. At this time, it is not clear which mechanism(s) contribute(s) to the increased Ti concentrations observed in SWPF solids.

3.5.2 Ferrous Alloy Solids

The origin of the ferrous alloy solids may be determined by calculating the ratio of elements potentially involved in such solids. For the sample data presented in Table 3-4, seemingly consistent ratios of Fe, Mn, Ni, and Cr can be calculated. The average ratios of iron to other elements are presented in Table 3-6, along with the ratio observed in common stainless-steel formulations.

Table 3-6. Ratios of Elements in Ferrous Alloy Solids From SWPF Samples and Common Stainless-Steel Formulations.

Ratio	SWPF Solids Average	304-L Stainless Steel[12]	316-L Stainless Steel[13]	17-4 PH Stainless Steel[14]
Fe/Cr	5.6	3.2 – 4.1	3.4 – 4.5	4.4 – 5.0
Fe/Mn	55.8	> 32.2	> 30.5	> 104
Fe/Ni	15.2	5.8 – 9.2	4.4 – 7.2	15.8 – 21.5

The data in Table 3-6 suggest that Fe:Cr ratios observed in SWPF solids are consistent with that observed in common stainless-steel components. This information, combined with the appearance of what appear to be shavings containing Fe, Mn, Ni, and Cr (see Figure 3-18 and Figure 3-22), is strongly indicative of metal particles due to component wear and erosion occurring within the SWPF. .

3.5.3 Alkali/Alkaline Earth-Containing Solids

As mentioned earlier, there is no solid evidence of separate particles made-up of alkali or alkaline earth metals other than a couple of localized SEM-EDS spectra with dominant calcium peaks. Given the correlation of alkali/alkaline earth metals is strongly correlated with sodium (a typically soluble alkali metal), it is believed that the presence of these species via ICP-AES is more likely tied to the supernatant concentrations of aqueous phases that have come into contact with the solids samples during or after formation. It is unclear to what extent the use of cleaning procedures during recovery of solid samples may impact these analyses. Furthermore, given the small concentrations of these metals in SWPF solids, it is unlikely that these species are as problematic for CSSX operations as those mentioned above (Hg-related and ferrous alloys).

3.5.4 Hardened Surface Solids

Given that the tungsten particles observed in EXT-007 solids (see Figure 3-7) are approximately 2-5 μm in diameter, it is likely that these particles were generated downstream of the alpha strike process filters within SWPF. The presence of tungsten and cobalt in SEM-EDS and ICP-AES data might indicate wear at components composed of W/Co-containing alloys (such as Stellite). Evidence of erosion of tungsten/cobalt-coated pump components in the presence of caustic supernatant streams has been seen in previous SRNL testing.[15] All of this information suggests that tungsten/cobalt-coatings and surfaces within the SWPF are likely experiencing erosion, leading to a slight contribution of solids build-up in CSSX processing. Note that the concentrations of W and Co in solid samples indicate that these solids are dwarfed by the other solids being generated (Hg-related and ferrous alloys). Note further that the potential presence of $MoWC_2$ (as indicated by XRD, see Figure 3-10 and Figure 3-25) might assist in identification of particular hardened surfaces of interest (those that also contain molybdenum).

3.5.5 Aluminum-Based Solids

The potential mechanisms for aluminum precipitation in the SWPF CSSX process are well established. Aluminum is believed to be present in CSS as sodium aluminate, or $NaAl(OH)_4$. Sodium aluminate is relatively soluble in caustic waste media, such as CSS. However, aluminum undergoes a chemical change upon neutralization to form insoluble aluminum hydroxides ($Al(OH)_3$) such as Gibbsite and Bayerite. As has been discussed, the potential for pH swings exists between the scrub and extraction contactors within the SWPF. Therefore, the observation of Gibbsite in SWPF solids (see Figure 3-9 and Figure 3-10) is consistent with the presence of aluminum in CSS and pH swings in CSSX.

An alternative mechanism for aluminum precipitation in SWPF CSSX contactors is the generation of sodium aluminosilicates. These insoluble species are known to form in caustic waste with elevated aluminum and silicon concentrations. The appearance Al and Si co-located in EDS spectra (see Figure 3-15) might indicate the presence of sodium aluminosilicate. It is therefore speculated that a small fraction of solids recovered from SWPF may be aluminum-based, with an undetermined mixture of Gibbsite and sodium aluminosilicates.

3.5.6 Salt Solids

The salt solids recovered from EXT-007 are also well understood with respect to SWPF operations. Sodium salts (such as carbonate, hydroxide, nitrate, nitrite, etc.) are fed to the CSSX extraction contactors as CSS. In cases where wetted components are allowed to dry (such as evaporation, level change, or cleaning), layers of these salt components would be expected to crystallize along drying surfaces. These solids would be expected to go into solution easily with rehydration and do not represent a large risk to SWPF processing. While no analyses of EXT-040-Top solids were performed, it is expected that these solids would exhibit similar properties and characteristics.

4.0 Conclusions

The following conclusions are offered as a result of this work.

- The light solids recovered from EXT-007 are consistent with crystallized, soluble salt components (such as sodium nitrate, sodium hydroxide, and sodium carbonate), all of which can be easily re-dissolved in process water and do not represent a threat to SWPF CSSX processing.
    - While the light solids from the top of EXT-040 were not analyzed, it is believed that they share similar characteristics to those recovered from EXT-007.
- The dark solids recovered from EXT-001, EXT-031, and the inside of EXT-040 appear to be complex, consisting of several different types of solids:
    - High concentrations of mercury (Hg, 40-75% by mass) partially present as elemental Hg are consistent with the precipitation of Hg^0/Hg^{2+} from Hg^+ species in pH swing conditions.

- Moderate concentrations of titanium (Ti, 2-7% by mass) are also present, often co-located with Hg. This is consistent with co-precipitation, entrainment, and/or amalgamation of Ti with Hg.
- Moderate concentrations of iron (Fe, 1-3% by mass) are observed in SWPF solids and are likely attributable to erosion of stainless-steel components within the CSSX process.
- Small concentrations of tungsten (W) and cobalt (Co, <1% by mass) are observed in SWPF solids. The presence of these solids is consistent with the erosion of components coated with W and Co (e.g., Stellite).
- Small concentrations of aluminum (Al, <1% by mass) are observed in the form of gibbsite and potentially sodium aluminosilicate. The presence of these compounds is likely attributable to the pH swing observed between the scrub and extraction cycles within the CSSX process.

5.0 Recommendations

The following recommendations are made as a result of this work.

- Testing should be performed to determine the chemical drivers, process, and mechanism of Hg precipitation in CSSX processing. Special care should be taken to include titanium in tests to evaluate the potential for co-precipitation, entrainment, and amalgamation.
- Hg-mitigation options that would minimize or eliminate risks of Hg precipitation and solids accumulation (e.g., Hg-absorption techniques, ion exchange/adsorbents, flowsheet changes, etc.) should be assessed.

6.0 References

1. Eldridge, K. R. *SRNL Study of Solids Collected from CSSX Extraction and Scrub Contactors 202 A/B and 201 O/P*; **X-TAR-J-00001, Rev. 0**; Savannah River Mission Completion: Aiken, SC, 2022

2. Parsons *SWPF Process Building Scrub Contactors EXT-202A/B P&ID*; **M-M6-J-0038, Rev. 8**; Parsons: Aiken, SC, 2019

3. Parsons *SWPF Process Building Solvent Extraction Contactors EXT-201O/P P&ID*; **M-M6-J-0037, Rev. 0**; Parsons: Aiken, SC, 2008

4. (a) Personal CommunicationEldridge, K. R., RE: Details on Contactor Solid Samples. Woodham, W. H., Ed. 2023; (b) Woodham, W. H. *Electronic Laboratory Notebook Entry - Analysis of Contactor Solids from SWPF*; **L7748-00442-05**; Savannah River National Laboratory: Aiken, SC, 2023

5. SCD-6, M. *SRS Alara Program*; **SCD-6, Rev. 2**; Savannah River Site: Aiken, SC, 2022

6. Procedure *Technical Reviews*; **Manual E7, Procedure 2.60, Rev. 20**; 2021

7. Procedure *Technical Reports*; **Manual E7, Procedure 3.60, Rev. 9**; 2021

8. (a) Oji, L. N.; Fondeur, F. *Characterization of the Soluble and Insoluble Portions of Solids from the Salt Waste Processing Facility Tank 201 and Tank 202 Samples*; **SRNL-STI-2022-00145, Rev. 2**; Savannah River National Laboratory: Aiken, SC, 2023; (b) Oji, L. N.; Woodham, W. H. *Characterization of Salt Waste Processing Facility August 2022 Tank 201 Sample*; **SRNL-STI-2023-00062, Rev. 0**; Savannah River National Laboratory: Aiken, SC, 2023 (Draft)

9. Peters, T. B. *Initial Analyses of Solids from the Extraction, Scrub Contactors and Tank 49H Variable Depth Samples*; **SRNL-L3100-2014-00121, Rev. 0**; Savannah River National Laboratory: Aiken, SC, 2014

10. Birk, J. P. Characteristic Reactions of Mercury Ions. https://chem.libretexts.org/Bookshelves/Analytical_Chemistry/Supplemental_Modules_(Analytical_Chemistry)/Qualitative_Analysis/Characteristic_Reactions_of_Select_Metal_Ions/Characteristic_Reactions_of_Mercury_Ions_(Hg^{2+}_and_Hg_2^{2+}) (accessed March 17, 2023).

11. Lentsch, R. D. *Test Report: Caustic-Side Solvent Extraction Full-Scale Test*; **P-RPT-J-00009, Rev. 0**; Parsons: 2008

12. Specification, *Steel, Corrosion-Resistant, Sheet, Strip, and Plate 19Cr - 9.5Ni (304L)*; **AMS5511, Rev. K**; 2019

13. Specification, *Steel, Corrosion and Heat-Resistant, Powder for Additive Manufacturing, 17Cr - 13Ni - 2.5Mo (316L)*; **AMS7037**; 2021

14. Specification, *Steel, Corrosion-Resistant, Investment Castings 16Cr - 4.1Ni - 0.28Cb - 3.2Cu Homogenization, Solution, and Precipitation Heat Treated 180 ksi Tensile Strength (17-4)*; **AMS5344, Rev. G**; 2019

15. Mickalonis, J. I.; Imrich, K. J.; Jenkins, C. F.; Wiersma, B. J. *Slurry Pump Compatibility Testing*; **WSRC-TR-2000-00004, Rev. 0**; Westinghouse Savannah River Company: Aiken, SC, 2000

Distribution:

alex.cozzi@srnl.doe.gov
william.bates@srnl.doe.gov
boyd.wiedenman@srnl.doe.gov
brady.lee@srnl.doe.gov
cj.bannochie@srnl.doe.gov
christine.langton@srnl.doe.gov
clint.gregory@srnl.doe.gov
connie.herman@srnl.doe.gov
daniel.mccabe@srnl.doe.gov
david.diprete@srnl.doe.gov
eric.skidmore@srnl.doe.gov
frank.pennebaker@srnl.doe.gov
William.Ramsey@SRNL.DOE.gov
gregg.morgan@srnl.doe.gov
heather.capogreco@srnl.doe.gov
holly.hall@srnl.doe.gov
joseph.manna@srnl.doe.gov
marion.cofer@srnl.doe.gov
marissa.reigel@srnl.doe.gov
mary.whitehead@srnl.doe.gov
michael.stone@srnl.doe.gov
morgana.whiteside@srnl.doe.gov
sarah.hodges@srnl.doe.gov
brent.gifford@srs.gov
clifford.conner@srs.gov
donna.yarbrough@srs.gov
glen.johnson@srs.gov
george.matis@srs.gov
james.somma@srs.gov
james.mullaney@srs.gov
justin.schulte@srs.gov
keith.sandroni@srs.gov
mark-l.johnson@srs.gov
myah.gaskins@srs.gov
Thomas.peters@srnl.doe.gov
steven.howell@srs.gov
thomas.burns@srs.gov
Ryan.lentsch@srs.gov
vijay.jain@srs.gov
Helen.Boyd@srs.gov
Wesley.Woodham@srnl.doe.gov
Drew.Fairchild@srnl.doe.gov
Elizabeth.Peck@srnl.doe.gov
Lawrence.oji@srnl.doe.gov